Chapter 3 Rock Properties

Rock properties are the measurable properties of rocks that are a measure of its ability to store and transport fluids, ionic species, and heat. Rock properties also include other measurable properties that aid in exploration or development of a reservoir.

Grain Size Distribution

Sieve Analysis

An easily measurable property of unconsolidated sand is the grain size distribution. The classical method for measuring grain size distribution is to use a set of sieve trays of graded mesh size as illustrated in Fig. 3.1.

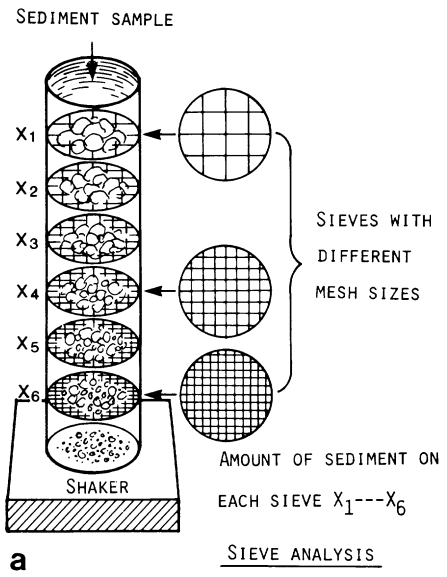

Fig. 3.1 Sieve analysis for measuring grain size distribution (Bjorlykke 1989)

The results of a sieve analysis are tabulated to show the mass fraction of each screen increment as a function of the mesh size of the increment. Since the particles on any one screen are passed by the screen immediately ahead of it, two numbers are needed to specify the size range of an increment, one for the screen through which the fraction passes and the other on which it is retained. Thus, the notation 14/20 means "through 14 mesh and on 20 mesh."

Table 3.1 Sieve analysis (McCabe, Smith, and Harriott, 1993)

Mesh	Screen opening d_i, mm	φ	Mass fraction retained x_i	Avg. particle diameter $\bar{d}_i$	Cum. mass fraction $\sum_i x_i$
4	4.699	-2.23			
6	3.327	-1.73		4.013	
8	2.362	-1.24		2.845	
10	1.651	-0.72		2.007	
14	1.168	-0.22		1.409	
20	0.833	+0.26		1.001	
28	0.589	+0.76		0.711	
35	0.417	+1.26		0.503	
48	0.295	+1.76		0.356	
65	0.208	+2.27		0.252	
100	0.147	+2.77		0.178	
150	0.104	+3.27		0.126	
200	0.074	+3.76		0.089	
Pan	0			0.037	

A typical sieve analysis is shown in Table 3.1. The first two columns give the mesh size and the width of the opening in the screen. The third column is the measured mass fraction retained on the designated screen. The fourth column is the average particle diameter retained in the corresponding mass fraction. The fifth column is the cumulative mass fraction coarser than the designated screen opening. Notice that the particle diameters differ by $\sqrt{2}$ or a φ increment of 0.5.

The classification of the sand into sand, silt, clay, or subdivision into coarse sand, medium sand, fine sand, ect. was shown in Fig. 2.5. Another scale that is sometimes. used rather than grain diameter in mm is the phi scale or the negative of the logarithm base 2 of the diameter in mm. Fig. 3.2 shows the correspondence between the two scales. This scale subdivides the different sand grain sizes between -1 to +4. The base 2 is because the Tyler mesh sizes sorts grain sizes by factors of 2 (see Fig. 2.5). Also, it is convenient to use a logarithmic scale because the distributions are usually approximately a log normal distribution.

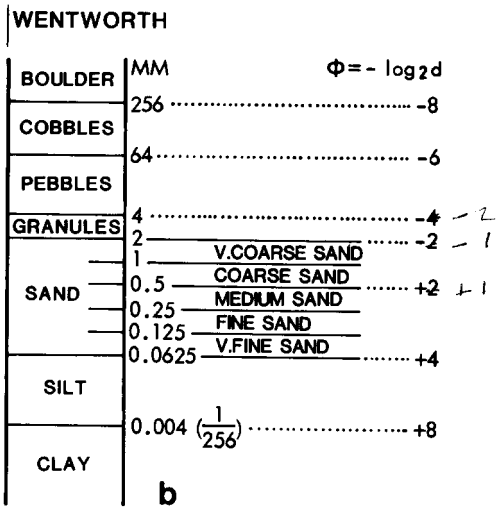

Fig. 3.2 Grain size classification of clastic sediments (Bjorlykke 1989)

Histogram

The simplest way to present the grain size distribution from a sieve analysis is to plot the weight retained on each tray as a histogram as in Fig. 3.3. A histogram shows what percentage by weight of the grains fall within a particular size range. This type of presentation gives a good visual impression of the distribution of grains in the various size categories. In particular, it is easy to see how well sorted the sediments are, and whether the distribution of grain sizes are symmetrical, or perhaps bimodal, i.e. with two maxima.

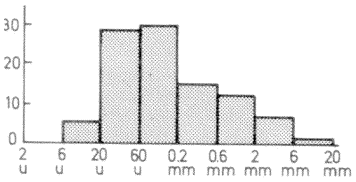

Fig 3.3 Histogram of grain size distribution (Bjorlykke 1989)

Cumulative Distribution

The cumulative grain size distribution in Fig. 3.4 shows what percent (by weight) of a sample is larger than a particular grain size. The steeper the curve, the better the sorting. The advantage of this type of display is that it allows easy fitting of discrete data and interpolation to read off particular values of the distribution. The grain size is plotted on logarithmic scale because the **logarithm** of the grain sizes often come close to being a normal or Gaussian distribution. A distribution of the logarithm of particle sizes may include many small particles but no negative size particles; which would be possible with a Gaussian distribution of particle sizes. A number of quantitative parameters can be determined from a cumulative distribution. These include the median, mean, skewness, and kurtosis. Formulas to calculate these quantities will be give later.

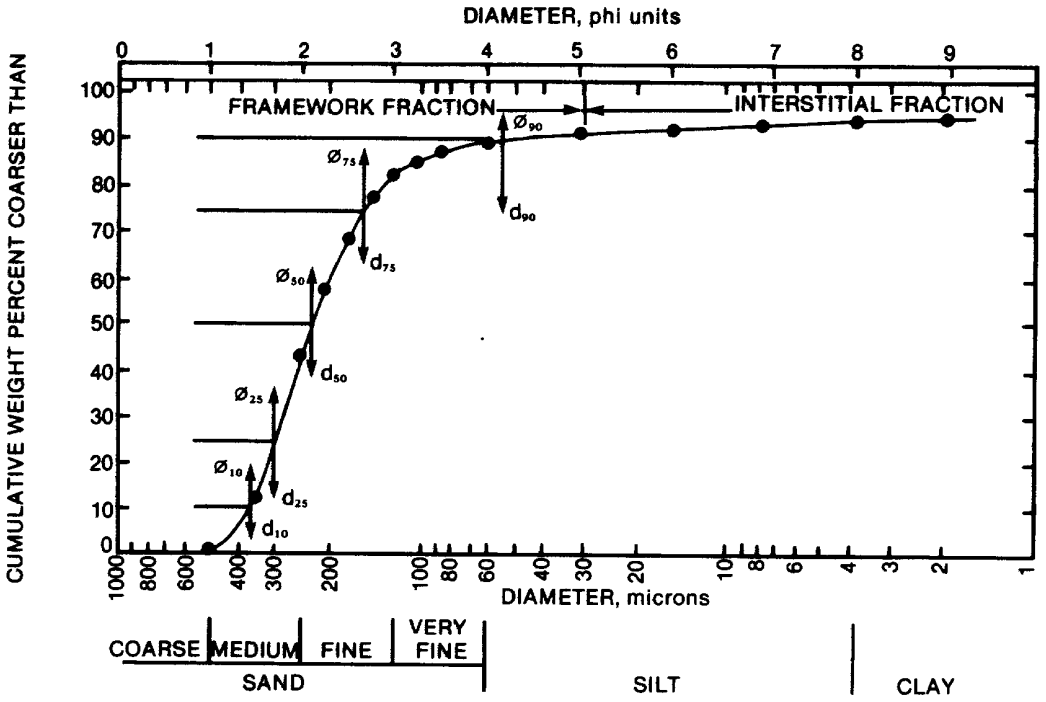

Fig. 3.4 Cumulative grain size distribution; percent by weight greater than a given diameter on a logarithm scale (Jorden and Campbell, 1984)

Phi Plot

We mentioned earlier than grain size distributions approximate a log-normal distribution. Thus a better approach to fitting data to a continuous distribution would be to plot the **logarithm** of the grain diameter from the sieve analysis on probability paper. A normal distribution will plot as a straight line on probability paper. The transformed grain diameter is the phi variable or $\varphi = -log_2 d$. Fig. 3.5 illustrates the grain size distribution on probability paper. Note that this transforms the larger grain sizes to the left and the distribution is given as percent larger than φ. Later we will examine log normal distributions using the natural logarithm.

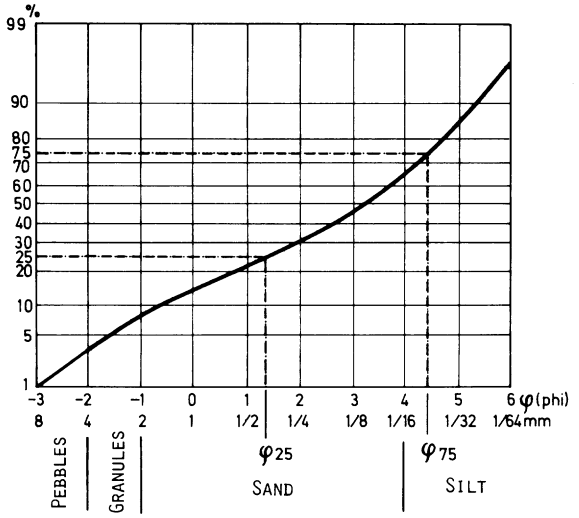

Fig. 3.5 A phi plot on probability paper (Bjorlykke 1989)

Grain Size distribution Parameters

The parameters of a millimeter plot or a phi plot can be determined from the following formulas (after Folk and Ward 1957 and Jorden and Campbell,1984.). φ_x is a grain size expressed in phi(φ) units such that x% of the sample is larger than this grain size. (Note: There are also other formulas to calculate the same quantity. Also, the definition of sorting does not appear to be consistent. Note: The mean with the φ scale is the geometric mean grain diameter.)

Scale	mm scale	φ scale
Mode:	*d* (most abundant class)	φ (most abundant class)
Median:	$\hat{d} = \mathrm{d}_{50}$	$M_d = \varphi_{50}$
Mean:		$M = \frac{\varphi_{16} + \varphi_{50} + \varphi_{84}}{3}$ or $\frac{\phi_{16} + \phi_{84}}{2}$
Sorting:	$S_o = \left[\frac{d_{25}}{d_{75}}\right]^{1/2}$	$S_o = \frac{\varphi_{84} - \varphi_{16}}{4} + \frac{\varphi_{95} - \varphi_5}{6.6}$
Skewness:	$S_k = \left[\frac{d_{25} \cdot d_{75}}{\hat{d}^2}\right]^{1/2}$	$S_k = \frac{\varphi_{16} + \varphi_{84} - \varphi_{50}}{2(\varphi_{84} - \varphi_{16})} + \frac{\varphi_5 + \varphi_{95} - 2\varphi_{50}}{2(\varphi_{95} - \varphi_5)}$
Kurtosis:	$K = \frac{d_{25} - d_{75}}{2(d_{90} - d_{10})}$	$K_g = \frac{\varphi_{95} - \varphi_5}{1.44(\varphi_{75} - \varphi_{25})}$

If the sample has a wide spread (tail) towards the fine grain sizes (larger phi values) and a relatively sharp delimitation at the large grain-size end, we say that the sample has positive skewness. Fig. 3.6 shows the range of sorting and skewness of deposits from different environments. Turbidite deposits have poor sorting because both coarse and fine materials get carried together in the under water mud slides. Eolian deposits have positive skewness (toward fines) because there is a upper limit to the size of grains carried by the wind but no lower limit. Beach sand has negative skewness (toward larger sizes) because wave action can transport large pebbles but the constant action of the moving water removes the fine particles.

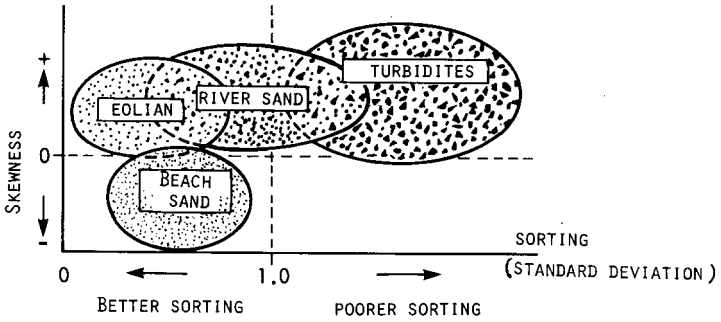

Fig. 3.6 Skewness and sorting for some depositional environments (Bjorlykke 1989)

Application of Grain Size Distributions

The grain size distribution can be used to estimate porosity and permeability if no other data is available. Fig. 3.7 illustrates such a correlation. This figure shows that the porosity is independent of grains size but is a function of sorting. Permeability is very much a function of the grain size but it also is a function of sorting. Since there is correlation of sorting and porosity, this figure implies that the permeability is a function of grain size and porosity. We will develop a model later to show this correlation. If the grains were geometrically similar (i.e., same sphericity and roundness), then the curves for sorting should be vertical and the curves for the different grain sizes should have the same shape.

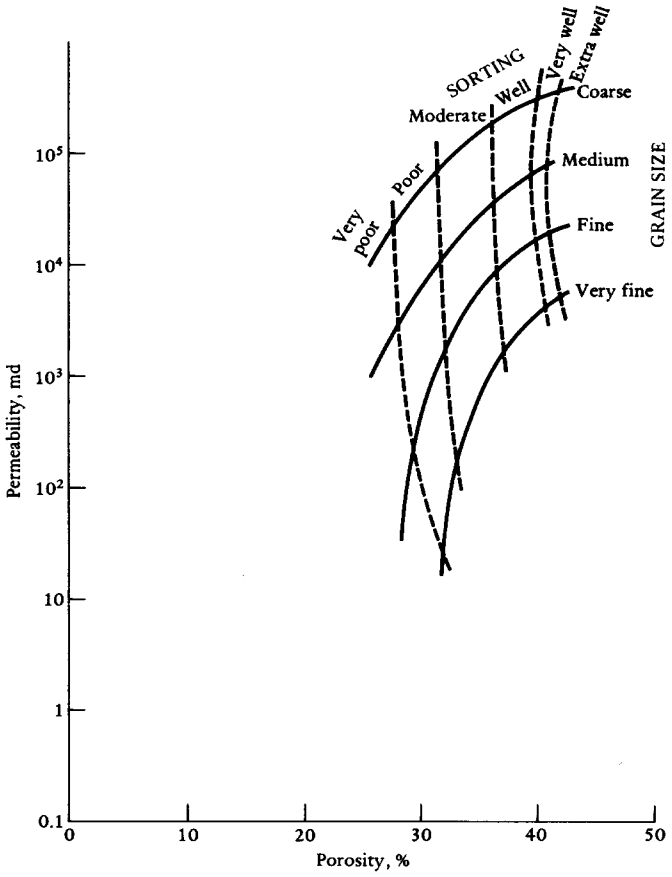

Fig 3.7 Porosity and permeability estimated from grain size distribution [Selley 1985 (Beard and Weyl 1973) and (Naggtegaal 1978)]

Quantitative measures of the grain size and sorting for the above figure are listed below (Beard and Weyl, 1973).

Size		Median Dia., mm
coarse	upper	1.000-0.710
	lower	0.710-0.500
medium	upper	0.500-0.350
	lower	0.350-0.250
fine	upper	0.250-0.177
	lower	0.177-0.125
very fine	upper	0.125-0.088
	lower	0.088-0.044

Sorting	S_o
extremely well sorted	1.0-1.1
very well sorted	1.1-1.2
well sorted	1.2-1.4
moderately sorted	1.4-2.0
poorly sorted	2.0-2.7
very poorly sorted	2.7-5.7

Fig. 3.8 illustrates different sorting for one value of median grain size. The article did not say how sorting was defined here.

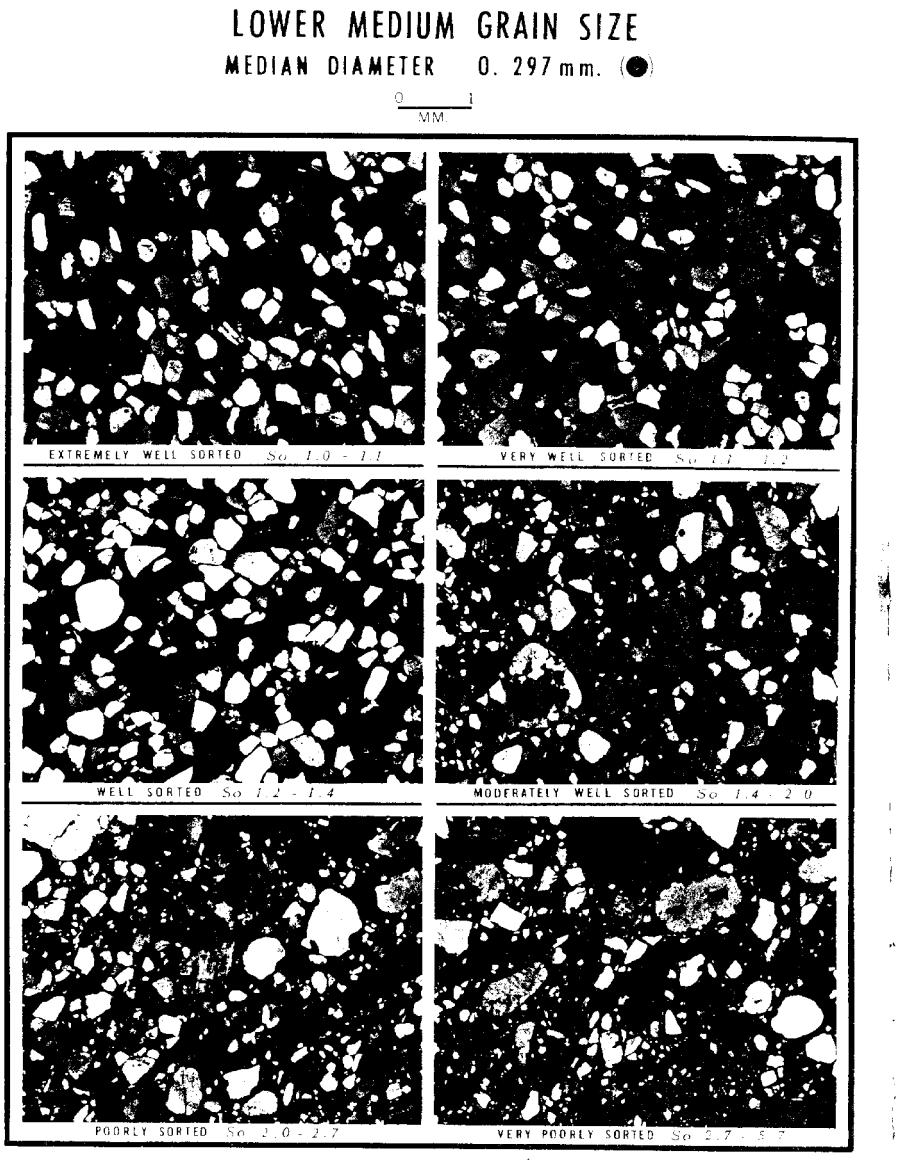

Fig. 3.8 Illustration of sorting viewed with dark field illumination microscopy that has been transformed to a binary (black or white) bitmap (Beard and Weyl, 1973)

Distribution Functions

The grain size distribution discussed above is the first of several random variables that will be encountered in this class. Other random variables that will be quantified are the pore size distribution, permeability distribution, and diffusion and dispersion processes. The grain size, pore size and permeability distributions are often approximated by a log normal distribution. In these cases the data can be fit to a log normal distribution and the properties of the distribution be expressed as simple functions with a few parameters. Also, thinking about random variables gives a foundation for the macroscopic variables such as capillary pressure curves, relative permeability curves, and fluid breakthrough curves.

Let x be a random variable from a large population such that it can be treated as a continuous variable. The histogram of x can then be expressed by a ***probability density function p{x}.*** The probability that an observation taken at random from a population with a density function $p\{x\}$ lies between x_a and x_b is as follows.

$$\Pr\{x_a < x < x_b\} = \int_{x_a}^{x_b} p\{x\}\, dx$$

It follow that :

$$\begin{aligned}\Pr\{x < x_b\} &= \Pr\{-\infty < x < x_b\} \\ &= \int_{-\infty}^{x_b} p\{x\}\, dx\end{aligned}$$

The ***cumulative distribution function P{x}*** is the probability that an observation from the population will be less than x_b.

$$\begin{aligned}P\{x\} &= \Pr\{x < x_b\} \\ &= \int_{-\infty}^{x_b} p\{x\}\, dx\end{aligned}$$

Also,

$$\frac{dP\{x\}}{dx} = p\{x\}$$

and

$$\begin{aligned}P\{\infty\} &= 1 \\ &= \int_{-\infty}^{\infty} p\{x\}\, dx\end{aligned}.$$

The relation between the probability density function and the cumulative probability density function is illustrated in Fig. 3.9.

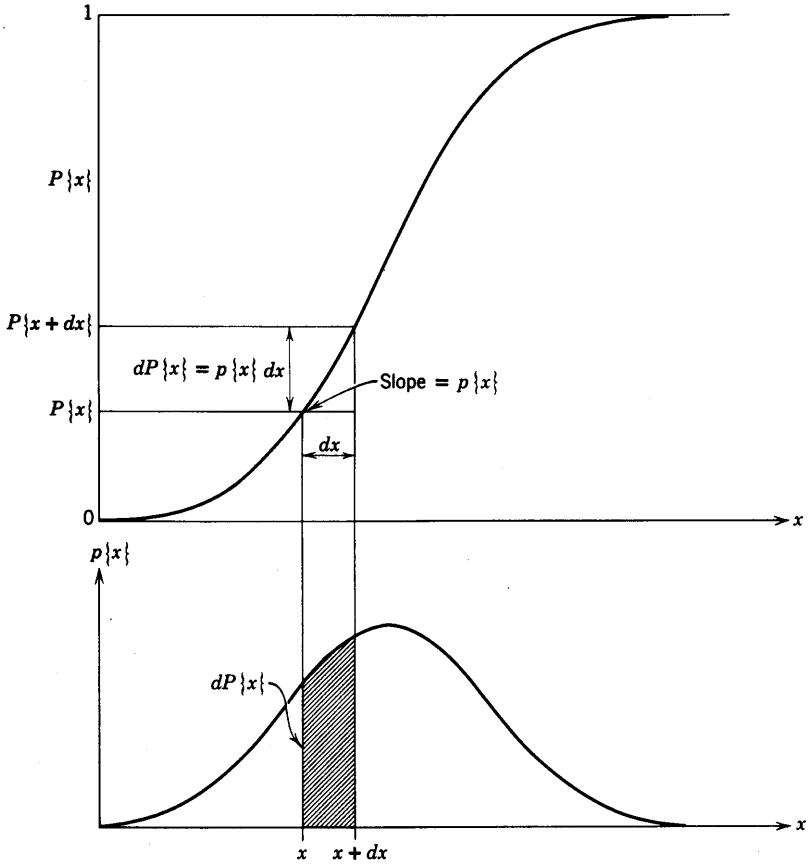

Fig. 3.9 Cumulative distribution function and probability density function (Brownlee, 1960)

Some parameters of the distribution:

X is a population of which *x* is a particular realization
p{x} is the probability density function of *x*
P{x} is the cumulative distribution function; *p{x} = dP{x}/dx*
mode: value of *x* at the maximum of *p{x}*
median: value of *x* where *P{x}*= 0.5

mean: expected value of *x*: $E(x) = \overline{x} = \int_{-\infty}^{\infty} xp\{x\}dx$

Variance: expected value of the square of the deviation of *x* from the mean: $V(x) = \int_{-\infty}^{\infty} (x - \overline{x})^2 p\{x\}dx$

standard deviation: square root of the variance, $\sigma = \sqrt{V(x)}$

Assignment No. 3.1 Properties of the Log-normal Distribution

Some random variables are well approximated by a log-normal distribution, i.e. the logarithm of the variable approximates a normal or Gaussian distribution. It is convenient to do analysis in terms of the standardized normal distribution which has a mean equal to zero and a variance equal to unity.

x is a random variable from a population X with a log-normal distribution.
$y = \ln x$; is a random variable from a population Y with a normal distribution.
$u = (y - \mu)/\sigma$, is a random variable with a standardized normal distribution.
Standardized normal distribution: $p\{u\} = \phi(u)$, $P\{u\} = \Phi(u)$.

$$\phi(u) = \frac{1}{\sqrt{2\pi}} e^{-u^2/2}$$

$$\Phi(u) = \int_{-\infty}^{u} \frac{1}{\sqrt{2\pi}} e^{-t^2/2}\, dt$$

$$= \frac{1}{2}\left[1 + \operatorname{erf}\left(\frac{u}{\sqrt{2}}\right)\right]$$

$P\{x\} = P\{x[y(u)]\}$; $P\{y\} = P\{y(u)\}$
Hint: $p\{x\} \neq p\{y\} \neq p\{u\}$

1. Derive formulas for: $p\{y\}$, $P\{y\}$, $p\{x\}$, $P\{x\}$

2. Express the mode, median, mean, and variance of U, Y, and X in terms of μ and σ. Present the results as a table.
Hint: Transform to functions of u before integrating.

3. What is the relation between the magnitudes of x_{mode}, x_{median}, and x_{mean}?

4. Plot $p\{u\}$ and $P\{u\}$.

5. Plot $p\{y\}$ and $P\{y\}$ for $\mu = 1.0$; $\sigma = 0.1, 1.0, 2.0$

6. Plot curves for $\mu = 1.0$; $\sigma = 0.1, 1.0, 2.0$
Variable: $p\{x\}$, $P\{x\}$
Scale: x, $\log_{10} x$, (i.e., semilog)
This is a total of 4 plots with three graphs per plot.

Pore Shape

The quantity of direct interest in the flow through porous media is not the properties of the matrix (e.g. grain size distribution) but rather the properties of the pores (e.g. pore size distribution). When we observe a porous medium, what we see is the matrix such as the beadpacks in Fig. 3.10. What we are interested in is the corresponding pore space as in Fig. 3.11.

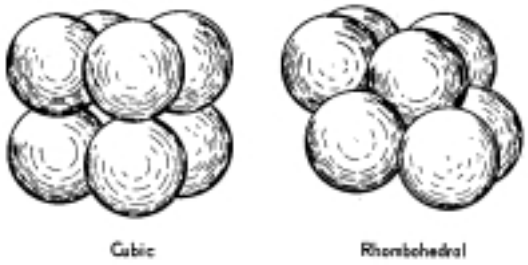

Fig. 3.10 Packs of spherical beads (Collins 1961)

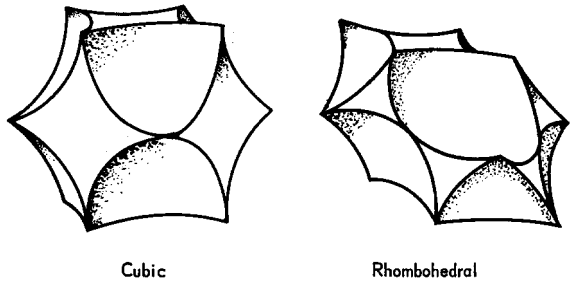

Fig 3.11 Pore space of spherical bead pack (Collins 1961)

It may be hard to visualize here but the cross sectional dimensions of the pore space will in general not be uniform as one moves through the pore space. In particular, there may be narrow passages called **pore throats** separated by wide passages called **pore bodies**. Fig. 3.12 attempts to distinguish between a throat and body.

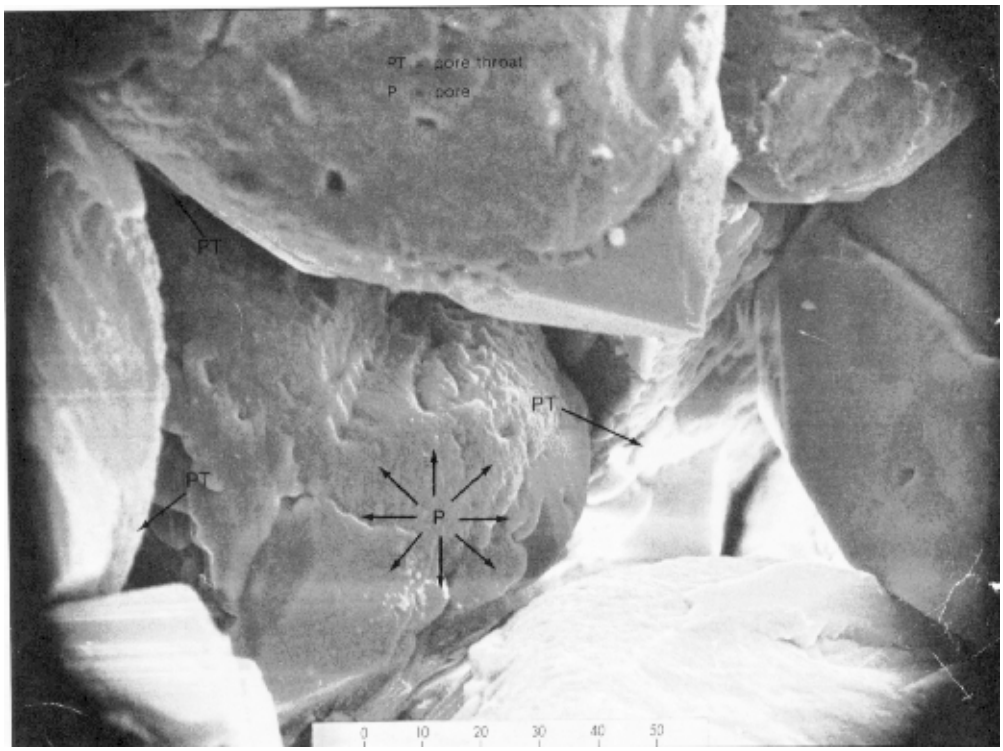

Fig. 3.12 SEM microphotograph of bore body and pore throat (Jordon 1984)

The pore space in rocks are much more complex than that of spherical bead packs. For example, Fig. 3.13 is a Wood's metal pore case of a consolidated sandstone. Important parameters of the pore space that relate to the trapping of fluids include the coordination number of the pores (i.e., the number of pore throats that branch out from a pore body) and the aspect ratio (i.e., ratio of pore body diameter to the pore throat diameter).

Fig. 3.13 Cast of pore space in sandstone (Collins 1961)

A common method for viewing the structure of the pore space is with thin sections. Here the rock is impregnated with dyed epoxy resin and sample is ground to a very thin slice. Fig. 3.14 is an example. Thin sections are routinely made for petrographic analysis. Minerals are identified from its morphology, staining with dyes, opaqueness, and appearance under crossed polarized filters. Grain size distribution and porosity can be determined by image analysis. Current research is attempting to estimate pore size distribution and permeability by image analysis.

Fig. 3.14 Thin section of a consolidated sandstone. The light areas are the sand grains. (Selly 1985)

Pore Size Distribution

Mercury porosimetry or mercury/air capillary pressure curves are commonly used to measure the distribution of pore throat sizes. A clean rock sample that may be irregular in shape (e.g., drill cutting) is placed in a high pressure vessel and is evacuated. Mercury is introduced into the vessel with small increments of pressure. The volume of mercury that goes into the vessel is precisely measured. The first volume of mercury fills the void space in the vessel. This will determine the bulk volume of the sample. Some mercury volume will then enter with increasing pressure to fill the surface roughness of the sample. The first volume of mercury to enter the rock will be at a pressure called the **capillary entry pressure** or **displacement pressure**. This is the pressure required for the mercury to enter the largest pores in the rock. The relation between the mercury pressure and the pore size that it will enter is illustrated by the following equation.

$$P_{Hg} = \frac{2\sigma_{Hg/air}\left(-\cos\theta\right)}{r_{pore}}$$

where

P_{Hg} is the mercury pressure
σ is the mercury surface tension
θ is the mercury/quartz/air contact angle ($\cong 140°$)
r is the pore throat radius

This equation treats a pore throat as having an equivalent pore radius. The mercury pressure is increased in small increments and the volume of mercury that enters is recorded. As the mercury pressure is increased, mercury enters pores that are accessible via smaller pore throats. The curve of mercury pressure versus mercury volume is called the mercury/air capillary pressure. The mercury volume may be normalized by the bulk sample volume to be expressed as a saturation. Usually, $1\text{-}S_{Hg}$ is plotted on the abscissa to represent the saturation of the wetting phase (, i.e. so the curve will have the same shape as when plotted as a function of the water saturation from a capillary diaphram or centrifuge measurement). These measurements are automated and are done on a routine basis.

Additional information can be determined about the pore structure by a sequence of mercury intrusion and withdrawal steps. Fig. 3.15 illustrates the pores that are filled with mercury during mercury intrusion to increasingly higher pressures and the disconnected drops of mercury that remain after the pressure is reduced to zero. The capillary pressure curves during these scanning loops may appear as in Fig. 3.16. This figure shows the hysteresis in saturation that occurs because of trapping of the nonwetting phase (mercury) in the pore bodies that are entered by mercury. This trapping would not have occured if the pore network was a bundle of parallel capillary tubes. This trapping is dependent on the pore body/pore throat aspect ratio. The trapping characteristics can be expressed as a curve of initial nonwetting phase saturation versus the residual nonwetting phase saturation as illustrated in Fig. 3.17.

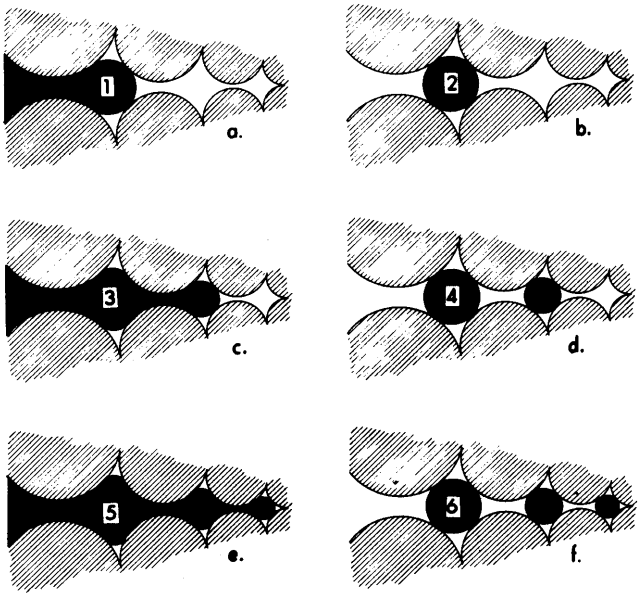

Fig. 3.15 Sequence of mercury injection and withdrawal. (Stegemeier, 1977)

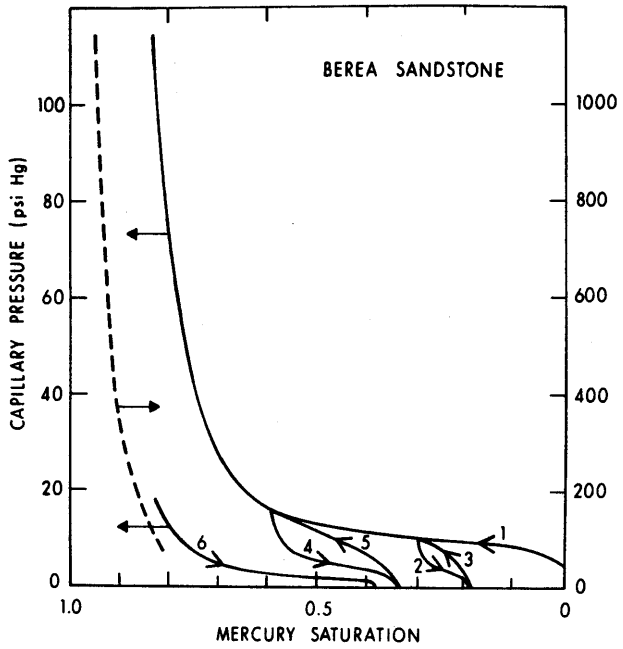

Fig. 3.16 Mercury intrusion-withdrawal curves (Stegemeier, 1977)

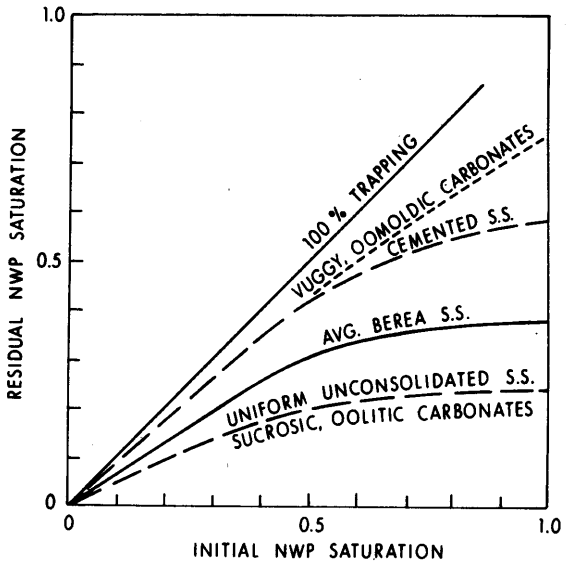

Fig. 3.17 Initial-residual saturation curves (Stegemeier, 1977)

Thomeer Model of the Capillary Pressure Curve

The mercury capillary pressure curve after correction for the entry pressure and the volumes normalized by the bulk sample volume may appear as in Fig. 3.18. The data is more useful if it can be reduced to a smaller set of parameters that characterize the rock. A model that is commonly (within Shell) used to parameterize capillary pressure data is the three parameter Thomeer model.

$$\frac{(V_b)_{P_c}}{(V_b)_{P_\infty}} = e^{-G/\mathrm{Log}(P_c/P_d)}$$

where

$(V_b)_{P\infty}$ is the fractional bulk volume occupied by mercury extrapolated to infinite mercury pressure, i.e., the total interconnected volume accessible to mercury.

P_d is the extrapolated mercury displacement pressure in psi, indicating the pressure required to enter the largest pore throat.

G is the pore geometric factor, reflecting the distribution of pore throats and their associated volumes. Note: G is defined with respect to Log_{10}. If $\log_e$ is used, then the parameter is $a = 2.303\,G$.

The convenient aspect of the Thomeer model is that it is a hyperbolic function on a log-log plot, Fig. 3.19. The parameters, P_d and $(V_b)_{P\infty}$, are estimated as the asympotes of a hyperboa passing through the data. The parameter G is adjusted to best fit the data.

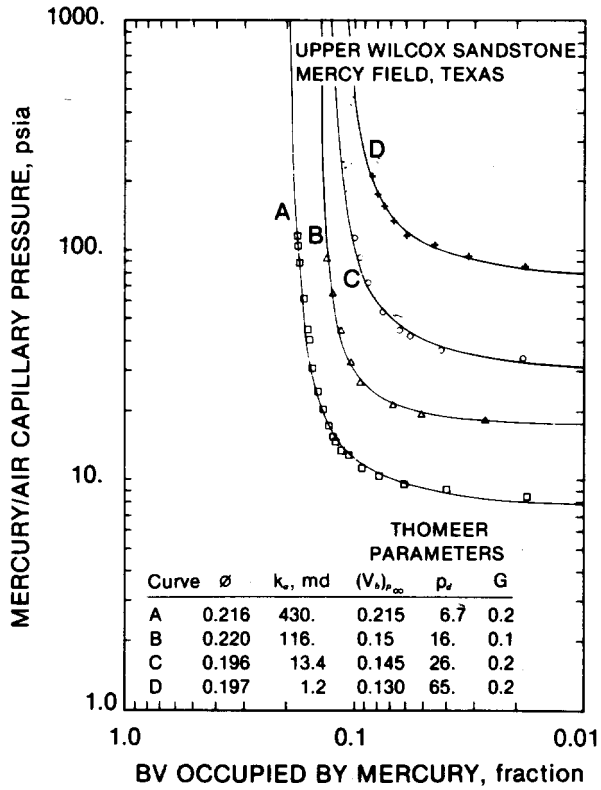

Fig. 3.18 Mercury/air capillarypressure curves (Jorden and Campbell, 1984)

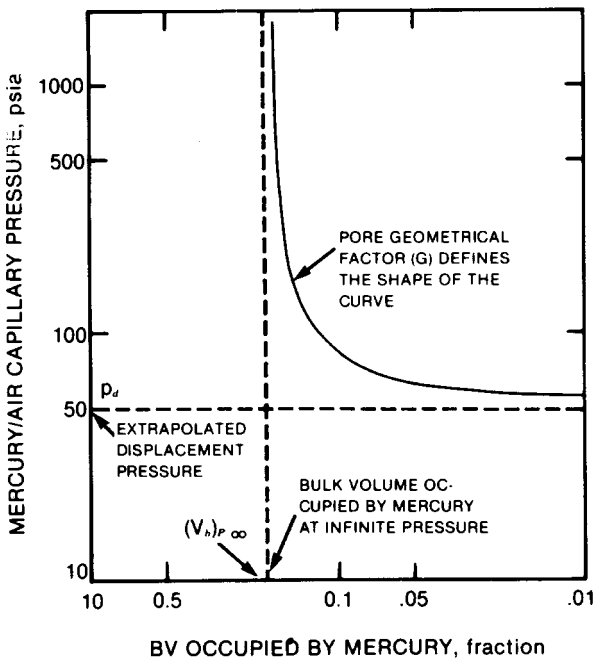

Fig. 3.19 Log-log plot for fitting mercury/air capillary pressure data with Thomeer model (Jorden and Campbell 1984)

Notice that $(V_b)_{P\infty}$ is close to the porosity, ϕ, for the highest permeability sample in Fig. 3.18 but is significantly less for the lower permeability samples. The Thomeer model does not recognize a bimodal pore size distribution and the discrepency may be due to the pore space between the clay particles. Bimodal pore size distributions occur when: (1) clays or other microporosity minerals are present, (2) in vuggy carbonates, (3) fractured rocks. Notice that the displacement pressure differs by an order of magnitude but there is little change in the pore geometrical parameter.

Fig. 3.20 illustrates capillary pressure curves of rocks with similar grain size and sorting but different types of dispersed clays. The "discrete particle" kaolinite acts as if they are another sand grain and has little effect on the permeability and the capillary pressure curve. The "pore lining" chlorite reduces the pore throat radius and thus increases the capillary pressure and reduces the permeability. The "pore bridging" chlorite spans the pore throats and thus greatly increases the capillary pressure and reduces the permeability. Notice that these clays have little effect on the porosity so this difference in permeability could not have been correlated with porosity.

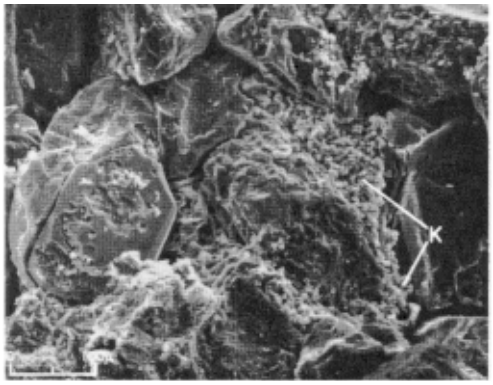

MIOCENE "S" SAND CONTAINING
"DISCRETE PARTICLE" KAOLINITE
ϕ = 22.9%
k_a = 1173 md.

TUSCALOOSA SAND CONTAINING
"PORE-LINING" CHLORITE (C)
ϕ = 25.7%
k_a = 41 md.

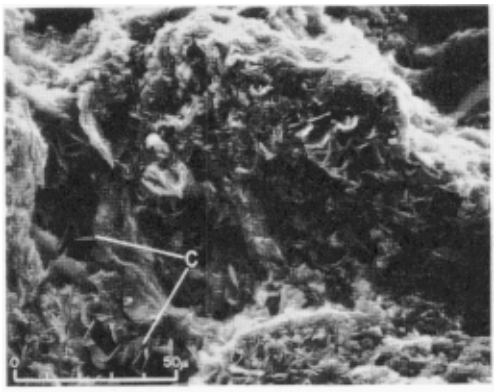

VICKSBURG SAND CONTAINING
"PORE-BRIDGING" CHLORITE (C)
ϕ = 19.1%
k_a = 0.09 md.

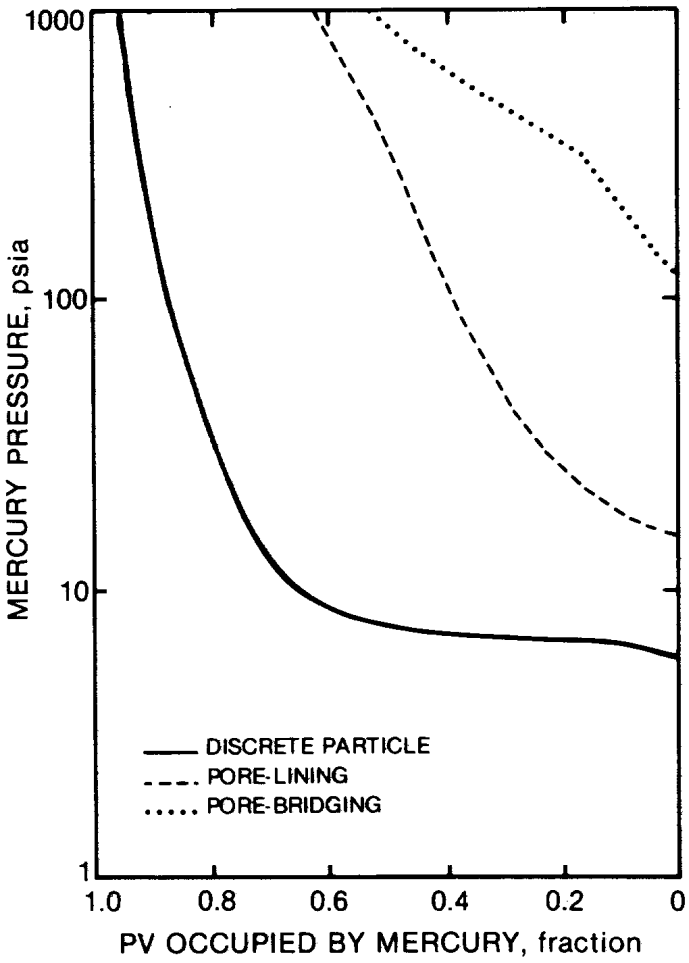

Fig. 3.20 Capillary pressure curves of samples with different pore structure (Jorden and Campbell 1984)

Assignment 3.2 Fitting Data with Thomeer Capillary Pressure Model

Estimate the Thomeer parameters for a Berea sandstone rock sample which has the mercury capillary pressure curve illustrated in Fig. 3.21. The saturation is expressed as water or wetting phase saturation rather than mercury saturation. The data and interpretation code is in owlnet and can be copied as *cp ~gjh/class/ thomd.dat* and *thom.m*. The output of the program appears as in Fig. 3.22 (for a poor set of parameters).

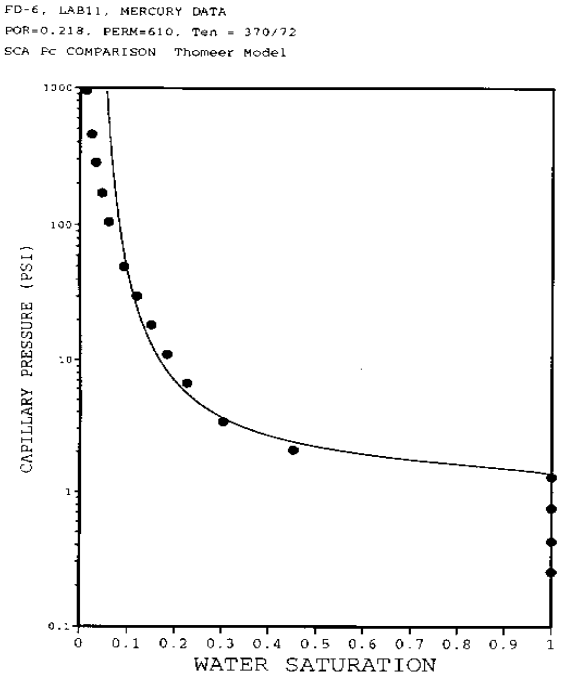

Fig. 3.21 Mercury/air capillary pressure data for Berea sandstone

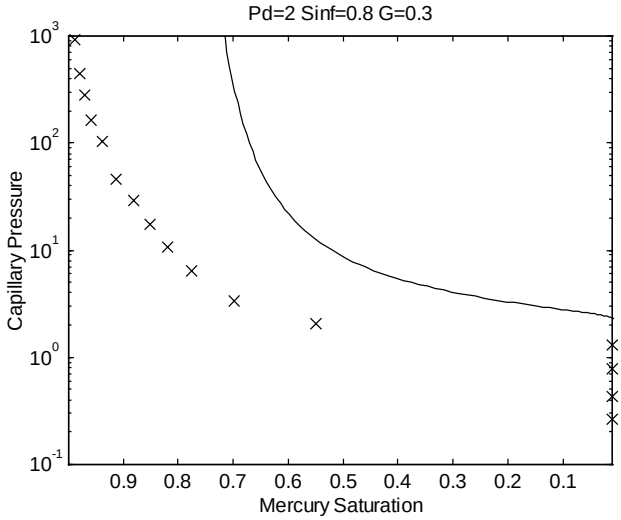

Fig. 3.22 Example output of thom.m

Fit of Capillary Pressure Data with Lognormal Distribution

While the Thomeer model is adequate for most rocks, there are cases where it does not adequately fit the capillary pressure data. Fig. 3.23 is an example of an Indiana limestone where the Thomeer model does not give a good fit. The lognormal distribution model works well in this case.

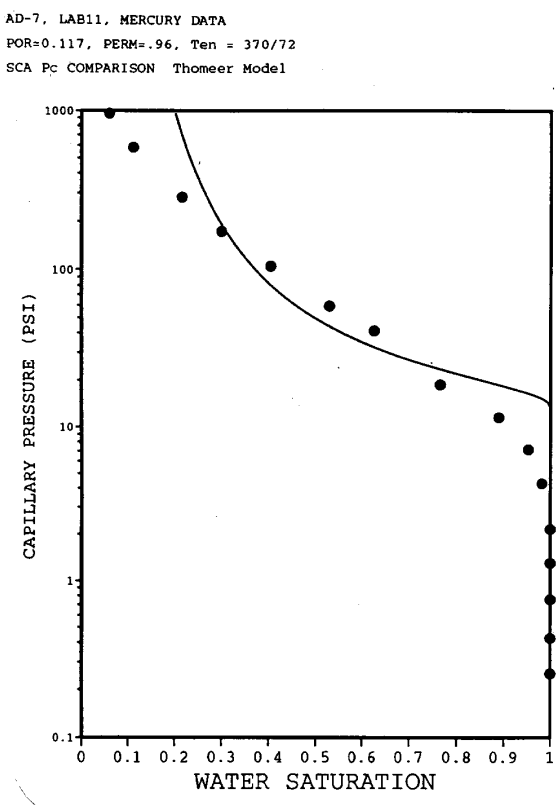

Fig 3.23 Mercury capillary pressure (points) and fit with Thomeer model (curve)

The traditional approach to fitting data to a Gaussian distribution has been to use probability paper. This is no longer necessary with computers and software to calculate the inverse error function and graph the results. In the following, suppose you are given sample measurements from a population that is approximated by the Gaussian distribution, P{y}, and you wish to find the mode, median, and mean (μ) and the standard deviation (σ) of the distribution. A Gaussian or normal distribution can be expressed as

$$\begin{aligned} P\{y\} &= P\{u(y)\} \\ &= \Phi(u) \\ &= \tfrac{1}{2}\left[1+\operatorname{erf}\left(u/\sqrt{2}\right)\right] \end{aligned}$$

where

$$u = (y-\mu)/\sigma$$

For the case of the distribution being the capillary pressure curve, *P{y}* corresponds to the cumulative fraction of the pore space occupied by mercury, or *1.0 -*S_w, if converted to wetting phase saturation. The variable y corresponds to the natural logarithm of the capillary pressure.

The parameters of the distribution, μ and σ, are to be estimated. The expression for the standard normal distribution can be inverted to express *u* as a function of *P{y}*.

$$u = \sqrt{2}\ \text{erfinv}\left[2P\{y\} - 1\right]$$

The function erfinv is the inverse error function which is available in MATLAB. The variable *y* is a linear function of *u*.

$$y = \mu + \sigma u$$

This equation can be expressed in terms of the measured variables, S_w and P_c.

$$\ln P_c = \mu + \sigma\, u\left(S_w\right)$$

This is a linear equation with slope σ and intercept μ. These parameters can be determined by linear regression.

The lognormal distribution as described here has the capillary pressure ranging from zero to infinity. Zero capillary pressure corresponds to a pore with an infinite radius of curvature. The model can be modified for finite pore sizes by including another parameter, P_d, the displacement or **capillary entry pressure** which is the capillary pressure below which the nonwetting phase will not enter the rock. The function that follows a lognormal distribution is then P_c - P_d for positive values. Also, the lognormal distribution as described here has the nonwetting saturation ranging from *0* to *1.0*. The distribution can be easily modified to be lognormal for nonwetting saturations between *0* and S_∞. Estimation of the parameters, P_d and S_∞ require either nonlinear regression or trial and error. Thus they will be neglected for now.

Assignment 3.3 Fit of capillary pressure data with lognormal model

Fit the data shown in Fig 3.23 with the lognormal distribution model. What are the estimated values for μ and σ? The data and code for fitting the data are available on owlnet as *~gjh/class/lime.dat lnorm1.m lnorm2.m gaussd.m gaussf.m cumpd.m*. Use the programs *gaussd.m* and *gaussf.m* to get familiar with fitting a Gaussian distribution. The program *lnorm1.m* converts the S_w vs. P_c data to a Gaussian distribution and *lnorm2.m* will plot the data and fitted distribution after the parameters are estimated with *gaussf.m*. The program *lnorm1.m* asks for *Nonwetting Sinf*. Use the program thom.m if you believe that it may have a value other than 1.0. Examine the fit of the data. Edit out data that you believe is dominated by noise. When fitting data in this manner, errors in P{y} near 0 and 1.0 may denominate the linear regression.

Pore Size from Capillary Pressure

The equation for the capillary pressure in a smooth capillary has the cosine of the contact angle in the expression. In the case of mercury on smooth quartz, the contact angle is 140°, measured through mercury. However, the pore walls in rocks is seldom smooth. Fig. 3.24 illustrates the apparent advancing and receding contact angles of fluids on rough surfaces. In mercury intrusion porosimetry, mercury is the nonwetting phase and air (vacuum) is the analog of a draining wetting phase. The contact angle measured through the wetting phase is then 180° - 140° = 40°. Fig. 3.24 the effective cos θ for a 40° contact angle is 1.0. Thus the factor for for cos θ is not needed for interpreting mercury-air capillary pressure in terms of the pore radius. However, not everyone is in agreement on this point.

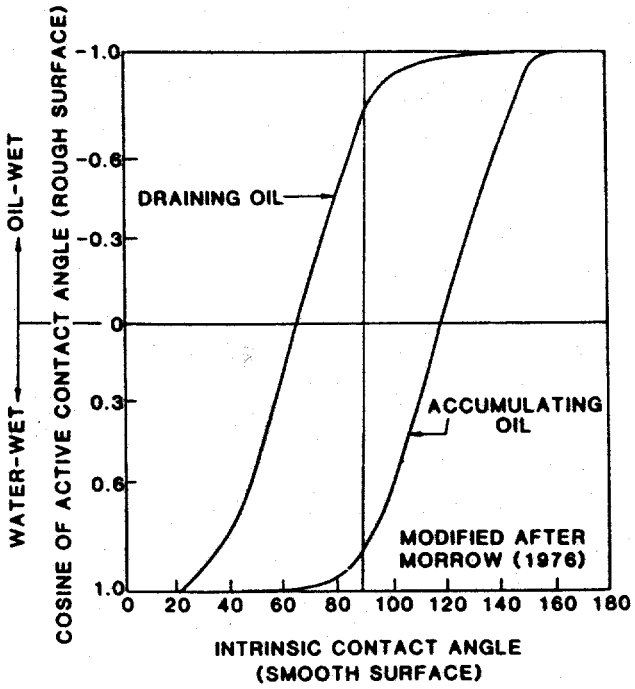

Fig. 3.24 Influence of surface roughness on effective cosine of contact angle. (Swanson 1985)

The expression for the capillary pressure in a smooth capillary tube is for a spherical surface in which twice the mean curvature is as follows.

$$P_c = \sigma \ 2H$$

If the mercury-air interface was confined between parallel plates, then one of the radii of curvature can be equal to infinity if the surface is translationally invariant. The mean curvature in this is as follows.

Microporosity and bimodal pore size distributions

The Thomeer and lognormal distributions are adequate for many systems but will fail to describe systems with a bimodal pore size distribution. Examples of bimodal distributions are (1) vuggy limestone consisting of the large pores (easily seen by the unaided eye) in the vugs and the matrix pores, (2) sandstones in which some particles are (micro) porous such as clay or chert particles, and (3) fractured rocks. Figure 3.25 and 3.26 are mercury porosimeter capillary pressure curve and incremental volume curve for a pore system with a trimodal character. The figures have been inverted so that the axis are in the same direction as the usual capillary pressure curves. The capillary pressure has been converted to capillary radii using the equation for the mercury capillary pressure in a straight capillary.

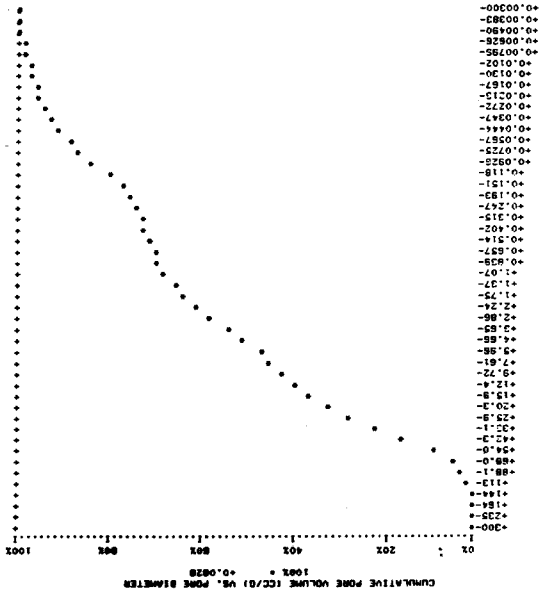

Fig. 3.25 Mercury capillary pressure curve expressed as pore radii (Swanson 1985)

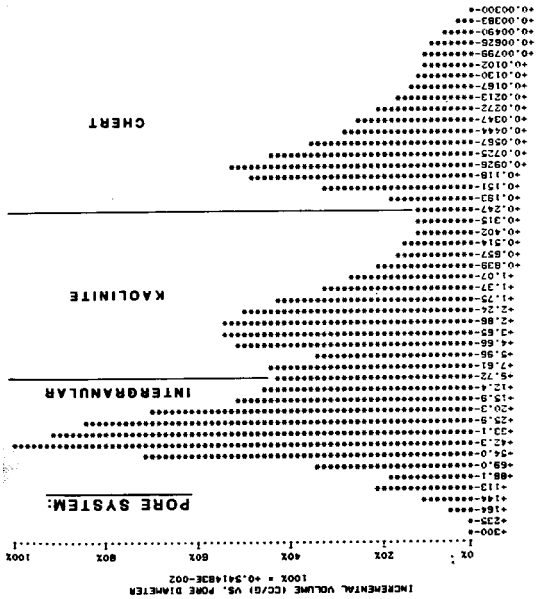

Fig. 3.26 Pore size distribution from incremental volume of mercury injection (Swanson 1985)

The capillary pressure curve appears to have several steps. When the data is expressed as incremental mercury volume, several peaks appear. (This is not a probability density curve) The peaks have been interpreted as the primary or intergranular pore system, kaolinite micropososity, and chert microporosity. The intergranular pore network which contributes the rock's permeability shows a peak in pore diameter at 42 μm. Kaolinite pore interconnections peak at about 3 μm, whereas the chert pores are much smaller, peaking at about 0.1 μm. The dip in pore diameter at 5.96 μm is associated with the instrument's pressure transition from low range to high range and is only an artifact.

Scanning electron microscopy (SEM) photographs of the kaolinite and chert particles are shown in Fig. 3.27 and 28. The pores in the kaolinite are far more plate-like than cylindrical. For a pore with large dimensions much larger than the small dimension, the calculated narrow dimension should be about half that computed for a cylindrical pore. From Fig. 3.26, the transition to mercury intrusion into the kaolinite begins at about 4.8 μm (one half of 9.7 μm). Intrusion continues over a broad size range to 1.5 μm (one half of 3 μm.) at the peak. This range of crystal spacing is comparable to the visual range observed in the SEM. The same comparison can be made for the porous chert.

Fig. 3.27 SEM of micropores in kaolinite. Note 10 μm scale. (Swanson 1985)

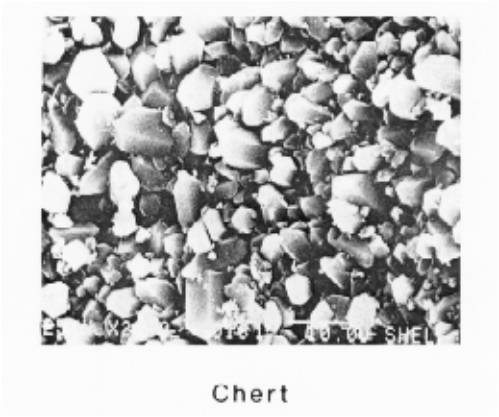

Fig. 3.28 SEM of micropores in chert. Note 10 μm scale. (Swanson 1985)

The example illustrated above show the importance of recognizing when there is more than one distribution of pore sizes. Fig. 3.29 is the mercury capillary pressure curve for a sandstone containing abundant chlorite. The **micropore** system is arbitrarily defined as pores with entry pressures greater than that found at the inflection point in the first steeply rising region of the capillary pressure curve. The **macropores** are those entered by mercury below this pressure. The latter contribute to hydrocarbon oil storage volume (oil saturation) and permeability.

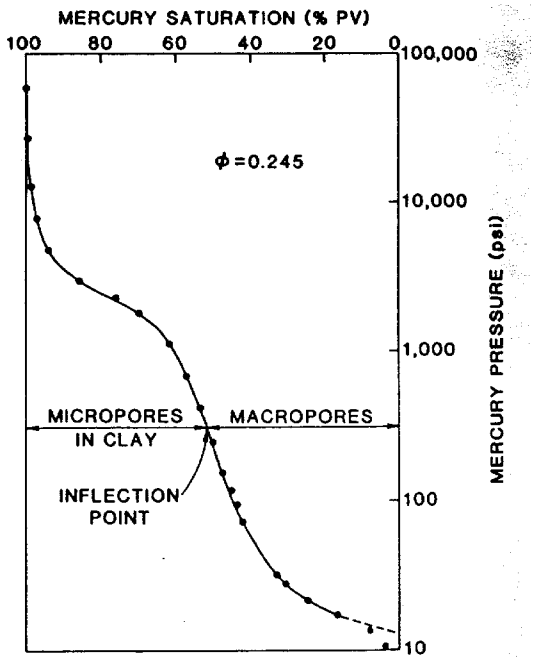

Fig. 3.29 Definition of microporosity from capillary pressure (Swanson 1985)

These examples of multipore systems show that the Thomeer and lognormal pore distribution models are not adequate for these systems. However, these models may be applied to the micro and macro porosity with a fraction distributing the porosity between the micro and macro porosity. Fig. 3.30 is an illustration of the bimodal lognormal model used to fit centrifuge capillary pressure measurements.

Model 6 - Lognormal - eight parameter

AC(1,6) Entry value for first lognormal
AC(2,6) Additional J value to reach second lognormal
AC(3,6) Additional J function to first peak
AC(4,6) Proportional to width of first peak
AC(5,6) Additional J function to second peak
AC(6,6) Proportional to width of second peak
AC(7,6) Denotes dominance of first peak

$\text{IF}(J \le AC(1,6))\,\text{THEN}$

$S1 = -1.0$

ELSE

$$arg1 = \frac{\ln\left[\left(J - AC(1,6)\right)/AC(3,6)\right]}{AC(4,6)}$$

$S1 = \text{erf}(arg1)$

END IF

$CJEH = AC(1,6) + AC(2,6)$

$\text{IF}(J \le CJEH)\,\text{THEN}$

$S2 = -1.0$

ELSE

$$arg2 = \frac{\ln\left[\left(J - CJEH\right)/AC(5,6)\right]}{AC(6,6)}$$

$S2 = \text{erf}(arg2)$

END IF

$$S(J) = \tfrac{1}{2}\left[1.0 - AC(7,6)\times S1 - \left(1.0 - AC(7,6)\right)\times S2\right]$$

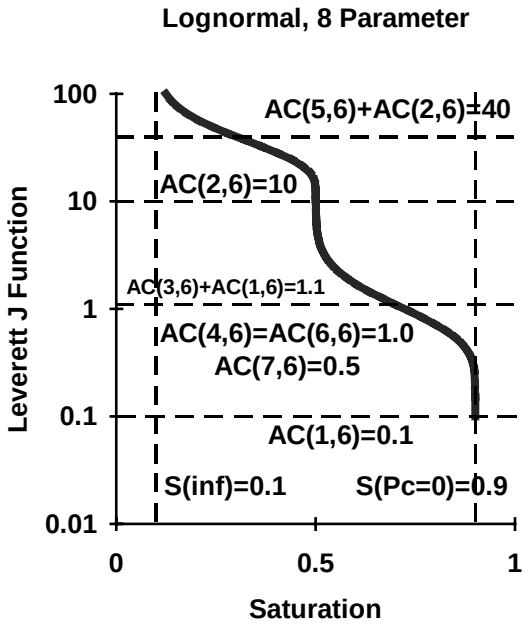

Fig. 3.30 Bimodal log normal distribution

Parameter	Value
$S(P_C=0)$	0.9
$S(P_C\to\infty)$	0.1
AC(1,6)	0.1
AC(2,6)	10.0
AC(3,6)	1.0
AC(4,6)	1.0
AC(5,6)	30.0
AC(6,6)	1.0
AC(7,6)	0.5

$$J(S) = \frac{0.2166}{\sigma}\sqrt{k/\phi}\ P_c(S)$$

$$S = \frac{\left(S_j - S_{j\infty}\right)}{\left(S_{ji} - S_{j\infty}\right)}$$

where
$J(S)$ is the Leverett J function
σ is the interfacial tension, dyne/cm or mJ/m^2.
k is the permeability, md
ϕ is the porosity, fraction
S is the reduced saturation
S_j is the saturation of phase j
S_{ji} is the initial saturation of phase j
$S_{j\infty}$ is the residual saturation or S(Pc$\rightarrow\infty$) of phase j

Surface Area

The specific surface area is a dominant parameter in models for permeability and in the transport of a species that can adsorb on the mineral surfaces. The specific surface area is usually expressed as square meters of surface per gram of solid. Here we will factor out the grain density and express the specific surface area as square meters per cubic centimeter of solid. (Later we will express the specific surface as a ratio of pore surface/pore volume.) The solid will be modeled as an oblate spheroid. This is a solid of revolution of an ellipse about its minor axis. The minor radius is *b* and the major radius is *a*.

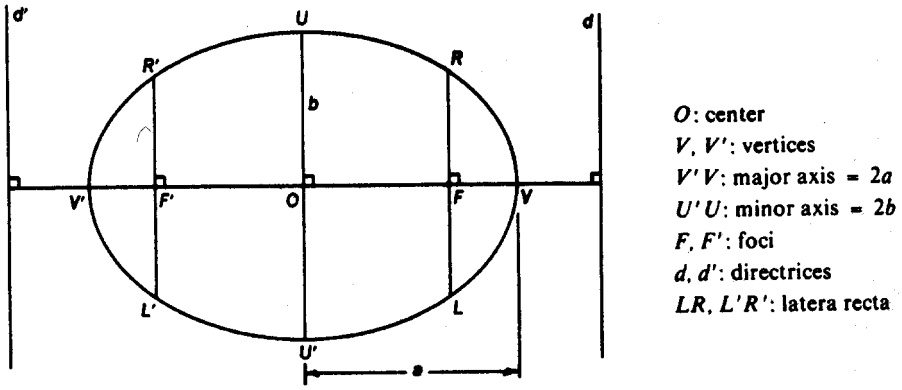

Fig. 3.31 Parameters of an ellipse (CRC Standard Mathematical Tables, 1987)

The ratio, *Sb/V*, is given by the following formula. (Mensuration formulas)

$$\left(\frac{S\,b}{V}\right)=\frac{3}{2}+\frac{3}{4}\left(\frac{1-\varepsilon^2}{\varepsilon}\right)\log_e\left(\frac{1+\varepsilon}{1-\varepsilon}\right)$$

where the eccentricity is

$$\varepsilon=\frac{\sqrt{a^2-b^2}}{a}$$

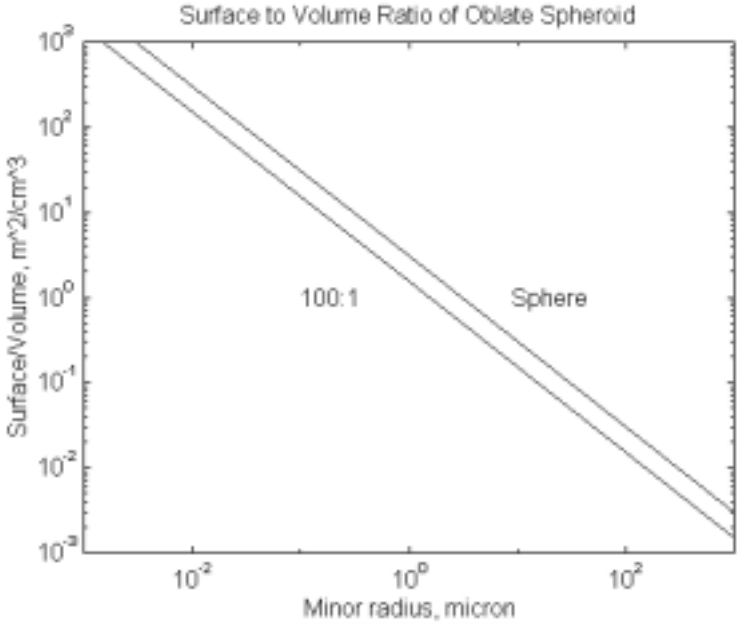

Fig 3.32 Surface to volume ratio of oblate spheroid

The group, *(Sb/V),* will have consistent units if *S* is in square meters, *V* is in cubic centimeters, and b is in microns. Figure 3.32 plots the specific surface as a function of the minor radius, *b*. The grain density (2.65 gm/cm^3 for quartz) has been factored out and the specific surface area is expressed as per unit cm^3 rather than gram. A upper coarse sand grain has a radius of about 10^3 microns

(one millimeter) and it has a surface area of about 10^{-3} m^2 /cm^3. A silt or clay particle with a minor radius of about 1.0 micron has a surface area of about 1.0 m^2/cm^3. A smectite sheet with a thickness of about 10^{-3} micron (1.0 nm) will have a surface area of about 10^3 m^2/cm^3. (Note: Is something is wrong here? The sphere appears to have a greater specific area than an oblate spheroid. A sphere should be a body of minimum area for a given volume. Answer: For the same volume, an oblate spheroid will have its surface to volume ratio increasing in proportion to the 2/3 power of the aspect ratio. The specific surface is plotted as a function of the radius of the minor axis. The major axis is greater than the minor axis ratio by the aspect ratio.)

When evaluating adsorption, the specific surface area of sand grains usually is not of much interest compared to the clays contained in the rock. For example the following table illustrates the range of specific areas that can be expected from clays (Corey 1990)

Clay type	Area, m^2/gram
kaolinite	45
illite	175
montmorillonite	800

In addition to the importance of the surface/volume ratio to adsorption on porous media, the ratio of surface area to pore volume will be shown later to be an important parameter in models of permeability and NMR relaxation of fluids in the pore space. The expression for the specific surface shows the surface to pore volume ratio to be inversely proportional to the length of the minor axis, *b*, for a given eccentricity. The constant of proportionality is 3 for a sphere and is equal to 3/2 for a thin disk. (Note: I think it should be 2 for a thin disk.)

Porosity

Porosity is the fraction (or percent) of the rock bulk volume occupied by pore space. The porosity may be divided into ***macro porosity*** and ***micro porosity*** in rocks that have a bimodal pore size distribution. Some examples include: (1) sandstones with a significant amount of clays, (2) sandstones with microporous chert grains, i.e., ***interparticle*** and ***intraparticle*** porosity, (3) carbonate rocks with vuggy porosity (caverns are an extreme case) and matrix porosity, (4) carbonate rocks with moldic porosity and matrix porosity, (5) carbonate rocks with interparticle porosity and intercrystalline porosity, (6) fracture porosity and matrix porosity. The total porosity can also be divided into ***effective*** porosity and ***ineffective*** porosity. Ineffective pores are pores with no openings or zero coordination number. Effective porosity can be divided into Cul-de-sac or dead-end pores with a coordination number of one and catenary pores with coordination number of two or more. These types of porosity are illustrated in Fig. 3.33.

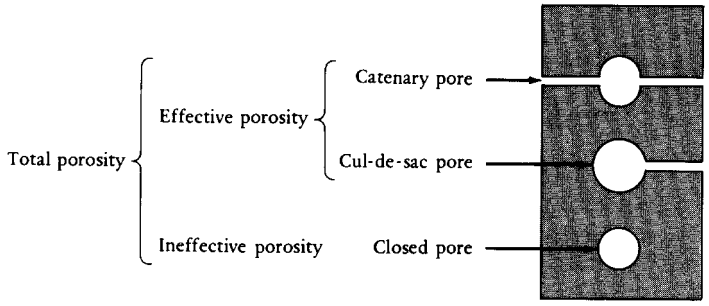

Fig. 3.33 The three basic types of porosity. (Selley 1985)

Sandstones

The rules for the factors governing the magnitude of the porosity is different for clastic (sandstone) and carbonate rocks. The following relationships between porosity and textural properties apply for sandstones (Jorden and Campbell 1984). Also see Fig. 3.7.

1. Porosity is independent of grain size for the same sorting.
2. Porosity decreases as sorting becomes poorer. See Fig. 3.7 and 3.34.
3. Porosity increases as grain sphericity (shape) decreases and as grain angularity (roundness) decreases. The general, though not universal, tendency is for diagenesis to reduce original porosity of clastic rocks.

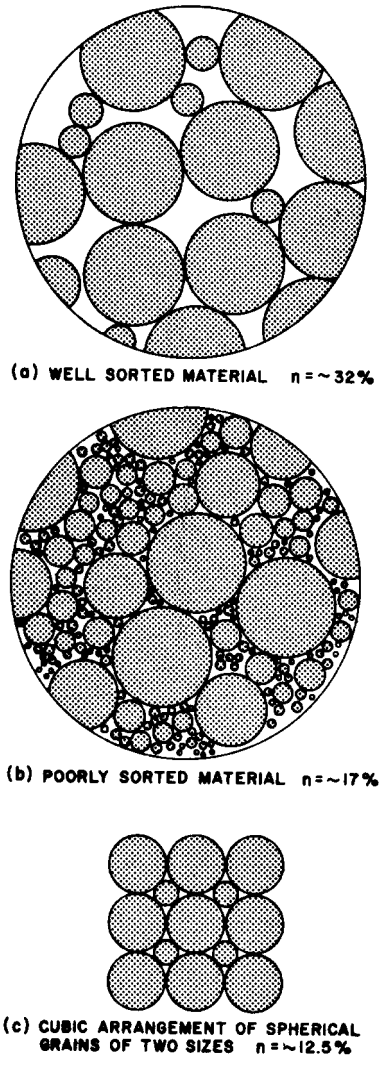

Fig. 3.34 Effect of sorting on porosity (Bear 1972)

The alteration of porosity through diagenesis is illustrated in Fig. 3.35. The porosity of the original sediment may originally be 40%-50%. In regions of rapid sedimentation such as in a river delta, ***compaction*** is the primary diagenetic alteration mechanism. Subsidence may accompany the compaction. Dissolution of some minerals and precipitation can result in consolidation of the rock and reduction of porosity by the process of ***cementation***.

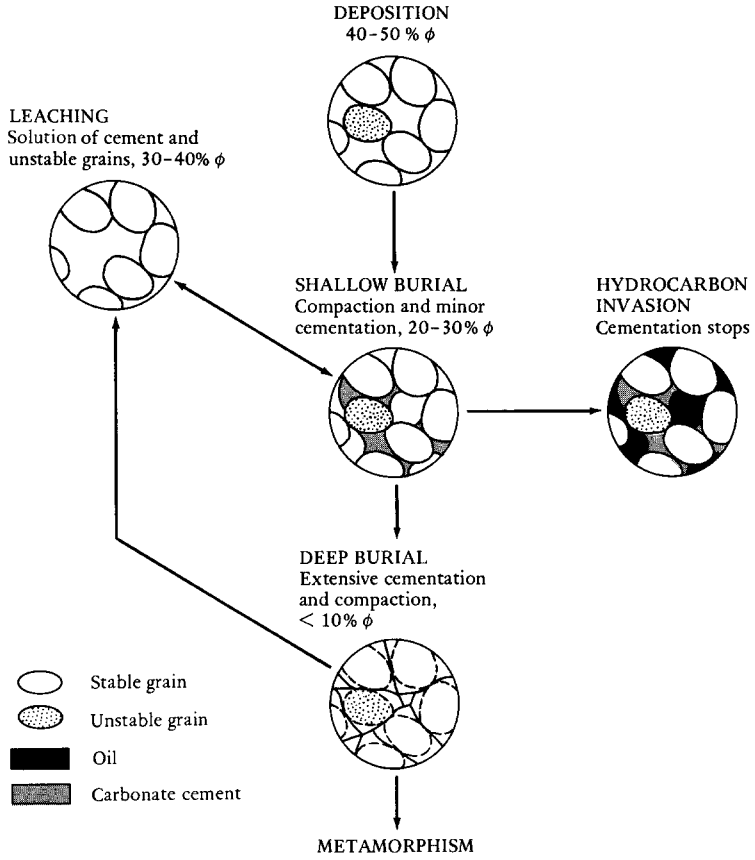

Fig. 3.35 Diagenetic pathways of sandstones (Selley, 1985)

Carbonate rocks

At deposition, carbonate sediments are highly to very highly porous. Some sediments have porosity ranging from 0.40 to 0.78 at deposition. The following relationships between porosity and textural properties apply to carbonates (Jorden and Campbell 1984).

1. Porosity is not correlated strongly with either median grain size or sorting.
2. Porosity is controlled largely by the amount of fines present -i.e., the larger the precent fines, the larger the porosity.
3. Diagenesis of carbonate rocks can result in porosity that is either significantly less or greater than original porosity.

Permeability

The mobility, denoted by λ, is a transport coefficient of the porous medium for the volumetric flux of a fluid just as electrical conductivity and thermal conductivity are transport coefficients for the flow of electrical current and heat, respectively. This transport coefficient was divided by Darcy into two factors ($\lambda = k/\mu$), the permeability, k, which is a property of the porous medium and the viscosity, μ, which is a property of the fluid. The permeability was originally conceived as a constant of a particular medium. However, in reality the permeability is generally not spatially uniform, i.e., porous media are usually heterogeneous, depends on direction, i.e., is not isotropic, depends on the current stress conditions and past stress history, is a function of the electrolyte composition of the fluids, and depends on the amount and distribution of the fluid phases, i.e., depends on relativity permeability. It is because of this highly variable nature of permeability that we need to know the factors that govern the value of permeability. We will describe two models of the permeability. They are both based on a bundle of capillary tubes model. However, one is based on a packed bed of spherical particles and the other is based on a pore size distribution model.

Packed Bed of Spherical Particles

One model for relating the flow resistance of porous media to the dimensions of the pores or particles is the Blake-Kozeny model (Bird, Stewart, and Lightfoot 1960). This model represents the pore network of the porous medium as a bundle of capillary tubes with an average or equivalent radius, *R*, and an average length, *L'*, that is somewhat longer than the system length. The effective radius is related to a particle diameter, D_p, by applying the hydraulic radius concept and assuming that the porous medium is a bed of uniform particles. The resulting expression is then compared with Darcy's law to determine an expression for the permeability of the medium in terms of the particle diameter and porosity.

Darcy's law is an empirical relationship between the flux and the driving force for laminar, single phase flow through porous media.

$$\begin{aligned} u &= q / A \\ &= -\lambda \frac{\Delta P}{L} \\ &= -\frac{k}{\mu}\frac{\Delta P}{L} \end{aligned}$$

where

$$P = p - \rho\, g\, z$$

The constant of proportionality between the flux and the driving force, commonly known as the *mobility*, λ, is directly proportional to the ***permeability*, *k*,** which is a property of the porous medium, and inversely proportional to the *viscosity,* μ, which is a property of the fluid.

The porous medium is modeled as a bundle of capillary tubes with a length *L'*, that is greater than the system length, *L*, due to the ***tortuosity*** of the pore network. $\tau = \left(L'/L\right)^2$ It has been empirically determined that this tortuosity factor can be approximated by the factor 25/12.

$$\tau = \left(L'/L\right)^2 = 25/12$$

The average velocity in a capillary tube is given by the Hagen-Poiseuille law.

$$< v >= \frac{R^2 \left(P_o - P_L\right)}{8\mu\, L'}$$

The average velocity in the bundle of tubes is greater than the average velocity in the pore space of the medium because of the greater length traversed in the tortuous capillary. Alternatively, it can be argued that the fluid it the porous medium must also traverse a greater length but the transverse components of velocity cancel in averaging over the porous medium and thus the average velocity in the pores of the medium is less than the average velocity in a tortuous capillary.

$$v_{pore} = \left\langle v \right\rangle_{capillary} \left(L / L'\right)$$

The average velocity of the fluid in the pores (***v**, the **interstitial velocity***) is related to the flux (***u**, **superficial velocity**, filtration velocity, or **Darcy velocity***) by the porosity of the porous medium (ϕ, pore volume/bulk volume). If the porous medium is random, then the fraction of the cross-sectional area open to pores is equal to the porosity. Thus the flux is

$$
\begin{aligned}
u &= \frac{q}{A} \\
&= \phi\, v \\
&= \phi < v > \left(L / L' \right) \\
&= \frac{\phi\, R^2 \left(P_o - P_L \right)}{8\mu\, L' \left(L' / L \right)} \\
&\frac{\phi\, R^2 \left(P_o - P_L \right)}{8\mu\, L\, \tau} \\
&= \frac{3\phi\, R^2 \left(P_o - P_L \right)}{50\mu\, L}, \qquad \tau = \frac{25}{12}
\end{aligned}
$$

By comparing the above equation with Darcy's law we have,

$$
\begin{aligned}
k &= \frac{3\phi\, R^2}{50} \\
R &= \sqrt{\frac{50k}{3\phi}}
\end{aligned}
$$

The above equation is an expression for the equivalent pore radius of the porous medium assuming a bundle of capillary tubes model with a tortuosity of 25/12.

The wetted surface of a porous medium can be related to the permeability and porosity by introducing the concept of the *hydraulic radius*. For flow in a capillary, the hydraulic radius is related to the radius as follows.

$$
\begin{aligned}
R_h &= \frac{\pi\, R^2}{2\pi\, R} \\
&= \frac{R}{2}
\end{aligned}
$$

In porous media, the hydraulic radius can be determined as follows:

$$
\begin{aligned}
R_h &= \frac{\text{cross section available for flow}}{\text{wetted primeter}} \\
&= \frac{\text{volume available for flow}}{\text{total wetted surface}} \\
&= \frac{\left(\text{volume of voids} \right) / \left(\text{volume of bed} \right)}{\left(\text{wetted surface} \right) / \left(\text{volume of bed} \right)} \\
&= \frac{\phi}{a}
\end{aligned}
$$

Note: The specific surface area in this equation is per bulk volume rather than grain volume as discussed earlier. We can eliminate the hydraulic radius between the last two equations to express the equivalent pore radius in terms of porosity and specific area.

$$R = \frac{2\phi}{a}$$

Substituting into the equation we derived earlier for the flux through a bundle of capillary tubes, we have

$$u = \frac{6\phi^3 \left(P_o - P_L\right)}{25 a^2 \mu L}$$

Comparing this equation with Darcy's law, we have

$$k = \frac{6\phi^3}{25a^2}$$

$$a = \sqrt{\frac{6\phi^3}{25k}}$$

This equation relates the wetted area of the porous medium to the permeability and porosity.

If we assume the porous medium to be a packed bed of uniform spheres, the particle diameter, D_p, can be related to the permeability and porosity. The specific area (per unit bulk volume) for a spherical bead pack with a porosity ϕ is

$$a = \frac{\pi D_p^2}{1/6\,\pi D_p^3}(1-\phi)$$

$$= \frac{6}{D_p}\left(1-\phi\right)$$

This specific area is the surface area per unit volume of bed. The surface area per unit volume of solid can be determined by dividing by the matrix volume/bed volume. This is the same as the ratio of the area and volume of a sphere.

$$\frac{a}{1-\phi} = \frac{6}{D_p}$$

By eliminating the specific area between the last two equations, we have an equation for the permeability as a function of the particle diameter.

$$k = \frac{\phi^3 D_p^2}{150(1-\phi)^2}$$

$$D_p = \sqrt{\frac{150(1-\phi)^2 k}{\phi^3}}$$

Symbols and conversion to consistent (SI) units (The SI Metric System of Units and SPE Metric Standard, SPE, 1984)

Quantity	Symbol	SI units	Customary units	multiply customary units by	
specific area (/ bulk vol)	*a*	m^2/m^3	m^2/cm^3	1.0	E+06
area	*A*	m^2	ft^2	9.2903	E-02
particle diameter	D_p	m	mm	1.0	E-03
			μm	1.0	E-06
permeability	*k*	m^2	μm^2	1.0	E-12
			darcy	9.8692	E-13
			md	9.8692	E-16
length	*L*	m	ft	3.048	E-01
pressure	*p*	Pa	kPa	1.0	E+03
			psi	6.8947	E+03
flow rate	*q*	m^3/s	cm^3/s	1.0	E-06
radius	*R*	m			
superficial velocity	*u*	m/s	ft/D	3.5278	E-06
interstitial velocity	*v*	m/s			
volume	*V*	m^3	ft^3	2.8317	E-02
			bbl	1.5899	E-01
viscosity	μ	Pa·s	cp	1.0	E-03
porosity	ϕ				
surface or interfacial tension	σ	N/m	mN/m	1.0	E-03
	σ	N/m	dyne/cm	1.0	E-03

The following table lists the permeability and porosity of some sand packs as a function of grain size and sorting.

Permeability (darcies) of artificially mixed and wet-packed sand [Jorden and Campbell 1984 (Beard and Weyl 1973)]

	Size							
	Coarse		Medium		Fine		Very Fine	
Sorting	Upper	Lower	Upper	Lower	Upper	Lower	Upper	Lower
Extremely well sorted	475.	238.	119.	59.	30.	15.	7.4	3.7
Very well sorted	458.	239.	115.	57.	29.	14.	7.2	3.6
Well sorted	302.	151.	76.	38.	19.	9.4	4.7	2.4
Moderately sorted	110.	55.	28.	14.	7.	3.5		

Poorly sorted	45.	23.	12.	6.
Very poorly sorted	14.	7.	3.5	

Porosity of artificially mixed and wet-packed sand [Jorden and Campbell 1984 (Beard and Weyl 1973)]

	Size							
	Coarse		Medium		Fine		Very Fine	
Sorting	Upper	Lower	Upper	Lower	Upper	Lower	Upper	Lower
Extremely well sorted	0.431	0.428	0.417	0.413	0.413	0.435	0.423	0.430
Very well sorted	0.408	0.415	0.402	0.402	0.398	0.408	0.412	0.418
Well sorted	0.380	0.384	0.381	0.388	0.391	0.397	0.402	0.398
Moderately sorted	0.324	0.333	0.342	0.349	0.339	0.343	0.356	0.331
Poorly sorted	0.271	0.298	0.315	0.313	0.304	0.310	0.305	0.342
Very poorly sorted	0.286	0.252	0.258	0.234	0.285	0.290	0.301	0.326

Assignment 3.4 Calculation of Permeability as a Function of Grain Size

Calculate and plot the permeability (darcy) as a function grain size (mm) and porosity for grain size in the range (10^{-4} mm to 10 mm) and porosity of (0.2, 0.3. 0.4, 0.5). Also plot the measured values for the extremely well sorted sand packs listed above. Post the average value of the sand pack porosity. Use Fig. 2.5 to determine the grain size. For a porosity of 0.4 tabulate the approximate grain size (in descriptive scale, mm, and μm) that will result in a permeability of 100 darcy, 1 darcy, and 1 md.

Estimation of Permeability from Pore Size Distribution

Rapid methods to estimate rock permeability has always been a high priority in the petroleum industry. Mercury porosimetry for measuring capillary pressure and calculation of permeability therefrom was introduced by Bob Purcell of Shell Oil Co. in 1949. The method treats the porous medium as a bundle of capillary tubes with the pore size distribution quantified by the mercury-air capillary pressure curve. The tortuosity is an empirical factor that brings the calculation into correspondence with measured permeability.

The average velocity in a capillary tube of radius R_i is described by the Hagen-Poiseuille law.

$$\langle v \rangle_i = \frac{R_i^2 \, \Delta P}{8 \mu \, L}$$

The capillary radius can be determined for the relation of the capillary pressure to an equivalent pore radius.

$$\left(P_c\right)_i = \frac{2\sigma \cos\theta}{R_i}, \qquad R_i = \frac{2\sigma \cos\theta}{\left(P_c\right)_i}$$

Thus the average velocity in a capillary tube can be expressed in terms of the capillary pressure at which that capillary is being entered be a nonwetting fluid.

$$\langle v \rangle_i = \frac{\left(\sigma \cos\theta\right)^2 \, \Delta P}{2 \mu \, L} \frac{1}{\left(P_c\right)_i^2}$$

Let $S(P_c)$ denote the fraction of the pore space that is occupied by the wetting phase when the capillary pressure is equal to P_c. Then dS is the incremental fraction of the pore space corresponding to P_c and P_c-dP_c. The interstitial velocity is the integral over all pores.

$$v = \int_0^1 \langle v \rangle \, dS$$

The superficial velocity (q/A) is then as follows.

$$u = \phi \, v = \frac{\left(\sigma \cos\theta\right)^2 \, \Delta P \phi}{2 \mu \, L} \int_0^1 \frac{dS}{P_c^2 \left(S\right)}$$

This equation can be compared with Darcy's law.

$$u = \frac{k}{\mu} \frac{\Delta P}{L}$$

By comparing the last two equation, an expression can be derived for the permeability.

$$k = \frac{(\sigma \cos\theta)^2 \phi}{2} \int_0^1 \frac{dS}{P_c^2(S)}$$

Tortuosity has not yet been considered to this point. Purcell introduced a factor, called the "lithology factor" to bring the calculated permeability into correspondence with the measured air permeability. We will use the tortuosity factor here to parallel the nomenclature for the packed bed.

$$k = \frac{(\sigma \cos\theta)^2 \phi}{2\tau} \int_0^1 \frac{dS}{P_c^2(S)}$$

Purcell observed that τ ranged from 2.8 for 1500 md sandstone to 12 for 1 md sandstone. This may be compared with the value of 25/12 $\approx$ 2 for a packed bed of spheres.

Thomeer (1960) refined the method by introducing a model for fitting the measured capillary pressure data.

Mercury capillary pressure curves can be measured from drill cuttings when cored samples are not available. Swanson (1981) observed that the low pressure portion of the capillary pressure curve was often different between measurements with small samples (e.g. drill cuttings) and larger core samples. This difference is thought to be due to the sample surface roughness and/or the accessibility of pores to the external surfaces. The low pressure portion corresponds the larger pores which contribute the most to permeability. Thus he suggested using a point on the capillary pressure curve that is independent of sample size. This point is the point of tangency of the curve of P_c versus mercury volume as a percent of bulk

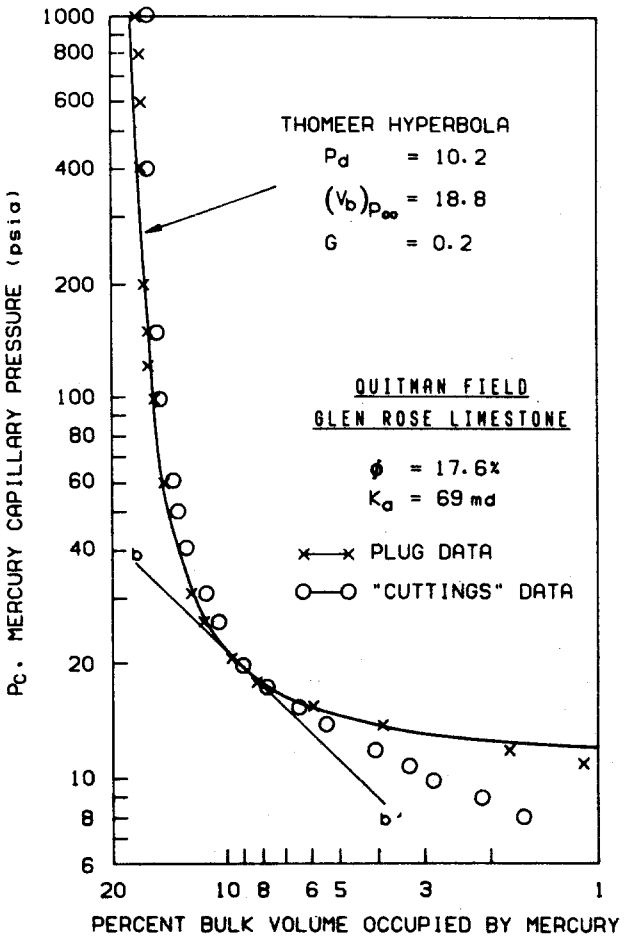

Fig. 3.36 Comparison of capillary pressure measured on plugs and cuttings (Swanson, 1981)

sample volume with the 45° line on a log-log scale. This method as well as the departure of the cuttings data is shown in Fig. 3.36. Using this method, the correlation for both clean sands and carbonates is as follows.

$$k_w = 355\left(\frac{S_b}{P_c}\right)_A^{2.005}$$

This correlation is compared with measurements in Fig. 3.37. In the event Thomeer parameters are known this equation can be expressed as follows.

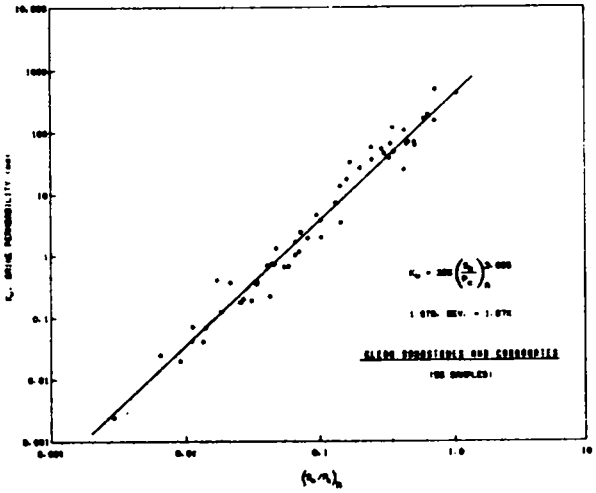

Fig. 3.37 Correlation of brine permeability with capillary pressure data (Swanson, 1981)

$$k_w = 355\left[10^{-2\sqrt{G/2.303}}\left(\frac{BV_{P\infty}}{P_d}\right)\right]^{2.005}$$

where

$BV_{P\infty}$ Thomeer percent bulk volume occupied by mercury at infinite mercury pressure (approximated by porosity)

G Thomeer pore geometrical factor

k_w brine permeability

P_c mercury capillary pressure, psi

P_d Thomeer mercury/air extrapolated displacement pressure, psi

S_b mercury saturation in percent of bulk volume (approximated by the product of porosity and mercury saturation)

$\left(S_b / P_c\right)_A$ correlating parameter taken at the point A (tangent to 45° line) of capillary pressure curve

Note that the exponent for this correlation agrees with the value predicted from Purcell's theoretical model using Poiseuille's equation. Ma, Jiang, and Morrow (1991) give a recent review of estimating the permeability from capillary pressure data.

Estimation of Permeability from Grain Size Distribution

We saw earlier (Beard and Weyl, 1973) that the parameters from the grain size distribution (grain size and sorting) has been used to correlate the porosity and permeability of clay-free unconsolidated sands. Now that we have a model (Kozeny) for the permeability, we are in a position do develop a correlation for predicting permeability from the grain size distribution.

Sorting. Sorting is usually expressed as qualitatively ranging from extremely well sorted to very poorly sorted. The earlier section on *Grain Size Distribution* listed the range of the sorting coefficient, S_o, that corresponds to the qualitative measure of sorting. Here we will use the arithmetic mean of the range to correspond to the qualitative measure of sorting. Now we will express the sorting in terms of the standard deviation, σ, of the distribution of the logarithm of the grain size. The sorting coefficient is defined as follows.

$$S_o = \left(d_{25} / d_{75} \right)^{1/2}$$

Assume that the grain size can be described by a log normal distribution. The grain size is then expressed as follows.

$$y = \log d$$

$$y = \mu + \sqrt{2}\,\sigma\,\mathrm{erfinv}\left[2P\{y\} - 1\right]$$

or

$$y = \mu + \sqrt{2}\,\sigma\,\mathrm{erfinv}\left[1 - 2P\{y\}\right]$$

where

- μ is the median of the distribution (log mean or geometric mean grain diameter)
- σ is the standard deviation of the log normal distribution

The choice of the two expressions depends on whether the cumulative probability corresponds to less than grain size *d* or greater than grain size *d*. The sorting coefficient is now expressed in terms of the logarithm of the grain diameter at the 25 and 75 percentile..

$$S_o = \exp\left(\frac{y_{25} - y_{75}}{2} \right)$$

$$y_{25} - y_{75} = \sqrt{2}\,\sigma\left[\mathrm{erfinv}(0.5) - \mathrm{erfinv}(-0.5)\right]$$

$$S_o = \exp\left(0.6744\,\sigma\right)$$

$$\sigma = \frac{\log S_o}{0.6744}$$

The transformation from the qualitative sorting, to the sorting coefficient (Beard and Weyl, 1973), and to the standard deviation of the log normal distribution is summarized in following table.

Sorting	S_o	σ
Extremely well sorted	1.05	0.072
Very well sorted	1.15	0.207
Well sorted	1.3	0.389
Moderately sorted	1.7	0.787
Poorly sorted	2.35	1.267
Very poorly sorted	4.2	2.128

Correlation of porosity with sorting. The porosity data of Beard and Weyl was correlated with the standard deviation (of the logarithm grain size distribution), Fig. 3.38.

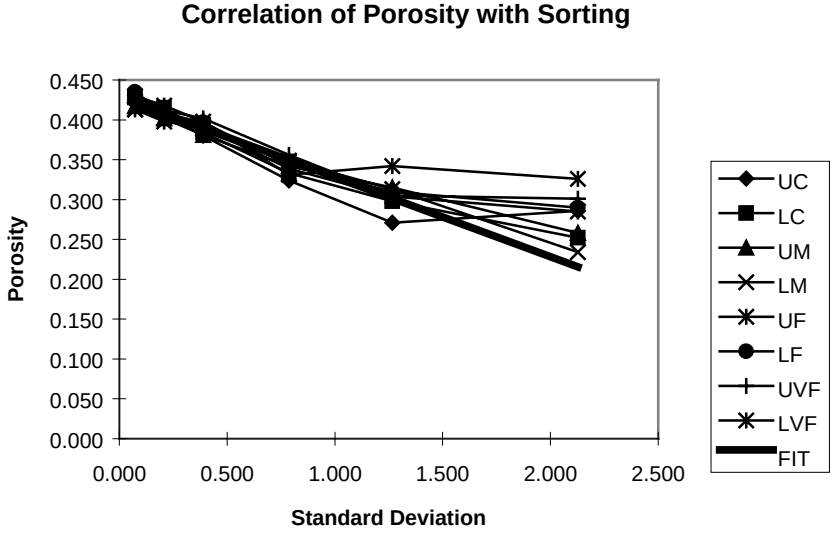

Fig. 3.38 Correlation of porosity with sorting (R^2 =0.93, excluding very poorly sorted data)

The regression of porosity with standard deviation excluding the *Very poorly sorted* data gives the following linear relationship.

$$\phi = 0.428 - 0.0998\sigma$$

Tortuosity. The Blake-Kozeny model determined a value of 25/12 for the tortuosity of a bed of uniform spherical particles. We will let the tortuosity, τ, be a function of the sorting. The Carman-Kozeny model is as follows.

$$k = \frac{\phi^3 \, D_p^2}{72\tau \left(1-\phi\right)^2}$$

or

$$\tau = \frac{\phi^3 \, D_p^2}{72k \left(1-\phi\right)^2}$$

Grain size	D_p
Upper coarse	1.30
Lower coarse	0.70
Upper medium	0.40
Lower medium	0.30
Upper fine	0.20
Lower fine	0.13
Upper very fine	0.10
Lower very fine	0.07

The tortuosity required to fit the Carman-Kozeny equation to the measured permeability of Beard and Weyl was calculated from the above equation. The grain size was estimated by transforming from the qualitative grain size to diameter in mm. The calculated tortuosity and the regression excluding the coarse sand data are illustrated in Fig. 3.39.

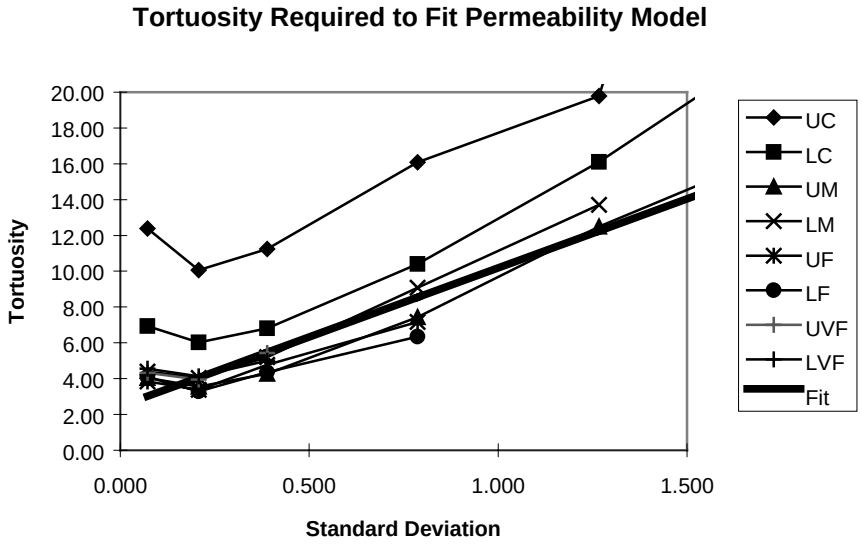

Fig. 3.39 Tortuosity required to fit Kozeny model for permeability (R^2=0.93, excluding coarse sand data)

Note that the tortuosity extrapolates to 2.5 for zero standard deviation, a value very close to the 25/12 determined by Blake for a spherical bead back. The linear regression, excluding the coarse sand data, give the following result.

$$\tau = 2.46 + 7.72\sigma$$

Since both the porosity and tortuosity are a function of the sorting, one would expect a cross-correlation between tortuosity and porosity. The cross-correlation of the linear correlations for porosity and tortuosity and of the porosity and tortuosity of the individual sands are shown in Fig. 3.40. The equation for the cross-correlation of the porosity and tortuosity correlations with sorting is as follows.

$$\tau = 35.6 - 77.3\phi$$

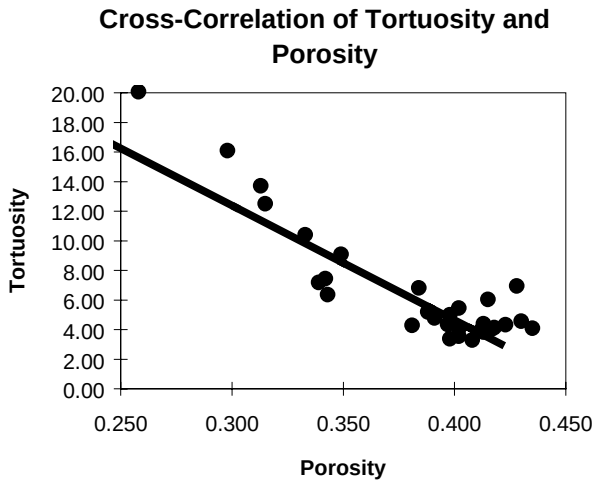

Fig. 3.40 Cross-correlation of porosity and tortuosity (upper coarse sand data omitted)

Permeability predicted from porosity, grain diameter, and sorting. The permeability predicted from the Carman-Kozeny model using the correlation for tortuosity given above is compared with the measured permeability of Beard and Weyl in Fig. 3.41. The predicted values for the upper coarse sand were much larger than the measured values and some are off the figure (i.e., >1000 darcy).

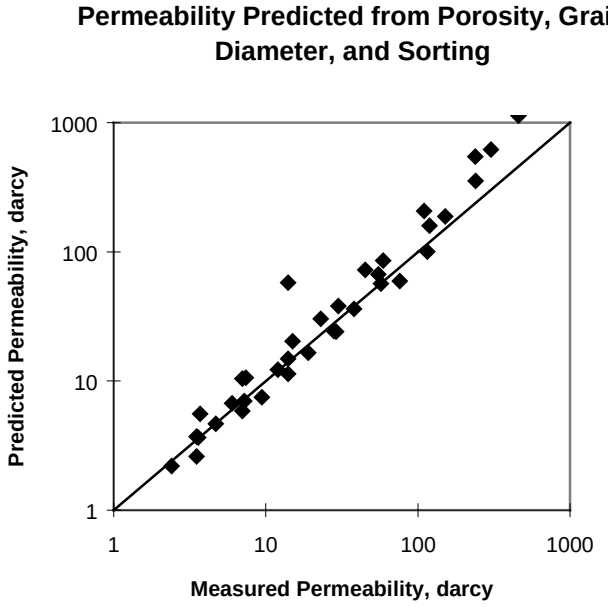

Fig. 3.41 Permeability predicted from porosity, grain size, and sorting (R^2=0.87)

If one has no other measurement other than the grain size distribution, then a measured porosity will not be available to use in the Kozeny model. In this case we can use the correlation of porosity with sorting derived above. The permeability correlated from the grain size and sorting is shown in Fig. 3.42.

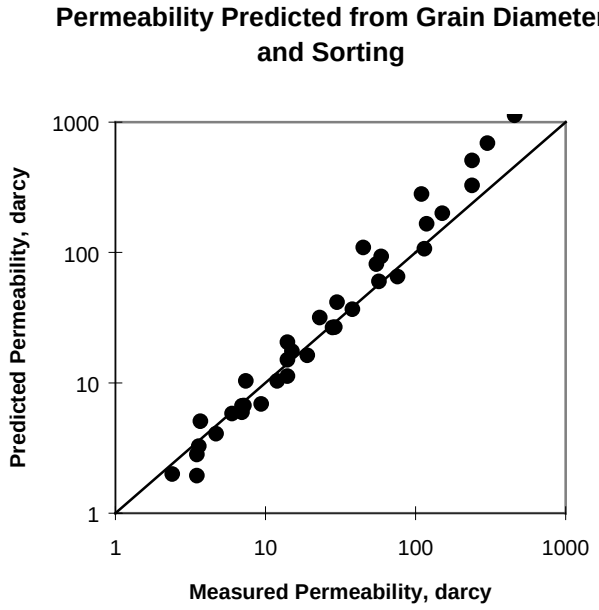

Fig. 3.42 Permeability predicted from the Kozeny model using only grain diameter and sorting (R^2=0.90)

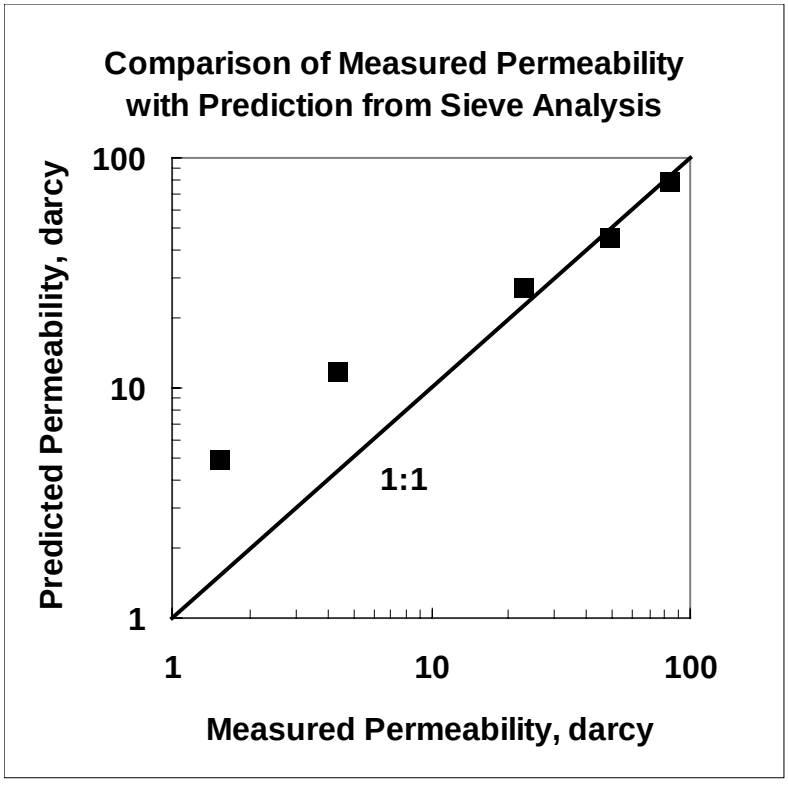

Independent test of correlation. The comparisons between measurement and prediction above are biased because the correlations were derived from the measurements. The correlations were used to predict the permeability distribution of an aquifer at Hill Air Force Base in Utah. Permeabilities were measured on selected samples to test the correlations. The comparison is shown in Fig. 3.43. The comparison is good for the high permeability samples but the deviation increases for the lower permeability samples. It was discovered that some of the samples containing clays had clumps of sand grains that were interpreted as a large sand grain. Thus the predicted permeability was too high for these samples. A clay sample was analyzed to have a median grain diameter of 1.11 mm. When the error was pointed out to the service company, they further pulverized the sample and reported a median grain diameter of 0.18 mm, apparently the result of only smaller clay aggregates. Thus sieve analysis of clay containing sediments will not be accurate without adequate pulverization of the aggregates.

Assignment 3.5 Estimation of permeability and porosity from sieve analysis.

Estimate the permeability and porosity of sample SB9-71 from the sieve analysis data the file in *~gjh/class/sb9-71.txt*. Cut and paste the grain diameter (in mm) and cumulative weight fraction data into a file with the sample name and an extension of *dat*. Process the data to estimate the median grain diameter and standard deviation with the MATLAB file, *~gjh/class/sieve2.m*. Show a plot of the fit of the lognormal distribution to the data. The measured values of permeability and porosity are 48.3 darcy and 0.395, respectively.

Other correlations. There is a frequent need to estimate permeability from grain size distribution. A survey of the literature has not been made here. Recently Panda and Lake (1994) estimated permeability from the grain size distribution. Unfortunately, they used the parameters of the distribution of grain diameter rather than the logarithm of the grain diameter. Their analysis is much more complex and they have to use a parameter for the skewness. A distribution that is a normal distribution (not skewed) in the logarithm of the grain size has skewed distribution of the grain size. Ostermeier (1995) recently developed a correlation using parameters of the grain size distribution (not the logarithm of grain size).

Effect of Stress on Porosity and Permeability

We discussed earlier how the porosity decreased with depth of burial. One of the factors in depth of burial is the increased stress that tends to compact the formation. The mechanisms discussed earlier were operating on a geological time scale (i.e., millions of years). Here we will consider mechanisms that operate on two time scales: (1) the producting life of a reservoir, and (2) the time scale of laboratory experiments.

The stress that is relavent to compaction of rock is the ***effective stress*** which is equal to the difference between the overburden stress or confining stress and the fluid pressure.The overburden stress is equal to the weight per unit area of overburden. The overburden may consist of e.g. 70% quartz with a density of 2.65 g/cm^3 and 30% brine of density somewhat over 1.0 g/cm^3. The confining stress can be hydrostatic (isotropic or equal in all three directions), triaxial (controlled stress in two or three directions), or uniaxial (stress applied in one direction and the sample confined in the other two directions).

The following is the result of a recent investigation on the effect of stress on the deep water Gulf of Mexico (GOM) turbidite formations (Ostermeier, 1993). Compaction is of serious concern for these reservoirs because the formations are unconsolidated or poorly consolidated, are highly geopressured (i.e., fluid pressure is greater than the hydrostatic water pressure for that depth), and water injection to maintain reservoir pressure may not be economically feasible for these reservoirs that are in sea depths greater than 1,000 feet. Compaction will impact several aspects of field operations. Seafloor subsidence may cause flooding in coastal areas or lowering of offshore platforms as in the case of the Ekofisk field. A compacting sand several tens of feet thick can impose damaging stress on production casing. Compaction can help maintain pressure during depletion by reduction of pore volume. However, compaction due to the low pressure around production wells can reduce the permeability and thus the production rate.

Fig. 3.44 illustrates the change of pore volume of a laboratory sample as a function of time for stress that is increased in steps. The pore volume decreases with increase in stress but it does not happen instantanously, i.e., there is creep or relaxation taking place. Fig. 3.45 shows the characteristic time for creep relaxation assuming a elastic-viscous model. The characteristic time is small compared to field depletion times but is significant compared to the time of laboratory experiments. Laboratory experiments should wait long enough at each stress to reach near equilibrium conditions.

Fig. 3.46 shows the pore volume compressibility as a function of the effective stress. Prospect A, which exhibits significant creep, shows a rapid increase in compressibility to rather large values with a subsequent hardening at higher applied stresses. Prospect D, which shows essentiall no creep has a low compressibility which actually decreases slightly with increasing stress. The creep and large compressibility observed for Prospects A and B arise from compressive and shear deformation of the *load bearing* softer grains. As applied stress increases, ductile grain yeild strength is exceeded and pore volume compressibility increases. With further increases in applied stress, the compressibility peaks at a relatively high value and begins to diminish as more of the load is taken up by the hard component. This hardening results from the gradual deformation or squeezing of the ductile material between hard grains and into

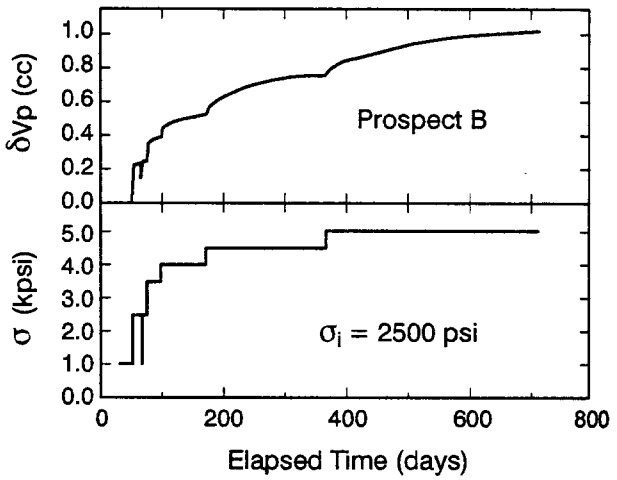

Fig. 3.44 Pore volume reduction in response to applied stress (Ostermeier 1993)

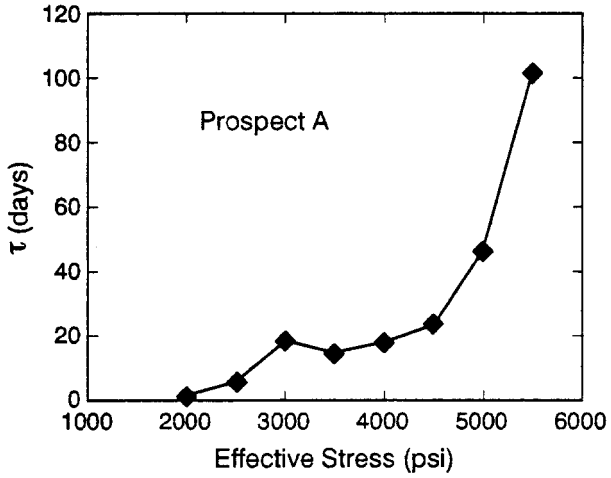

Fig 3.45 Creep rexalation time, τ, versus effective stress (Ostermeier 1993)

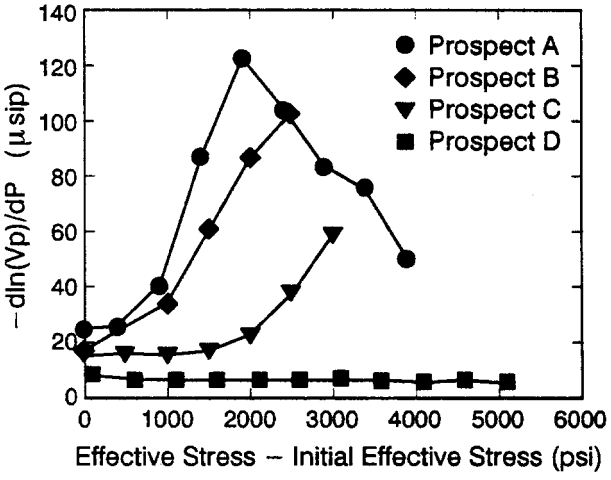

Fig 3.46 Pore volume compressibility versus effective stress (Ostermeier 1993)

intergranular areas. The Prospect D sample shows no softening. Though this sample contains ductile materials, this material is not load bearing at initial in situ conditions nor does it become so. Prospect D had deeper burial and greater in situ stress history compared to Prospect A and the ductile material apparently is no longer load bearing.

The cumulative effect of the pore compressibility is shown in Fig. 3.47. This shows that up to 8% reduction in pore volume can occur with a 4,000 psi increase in effective stress if the mineral type and distribution and the stress history are right.

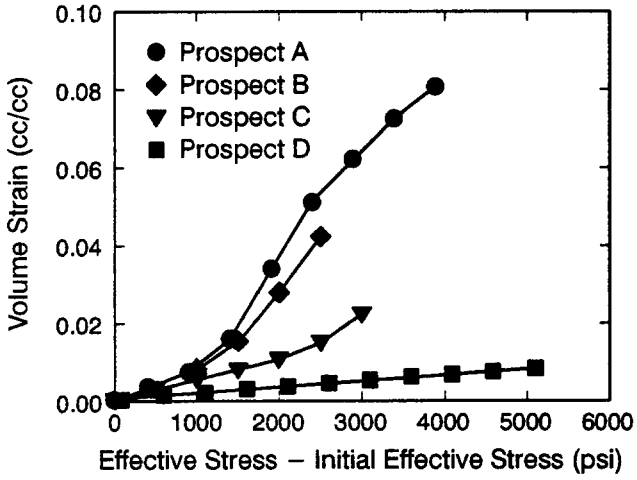

Fig. 3.47 Volume strain versus effective stress (Ostermeier 1993)

The permeability can decrease in correspondance with the reduction in porosity as shown in Fig. 3.48. The permeability in prospect A decreased to less than one third of its initial value. The permeability correlates with the reduction in porosity as shown in Fig 3.49.

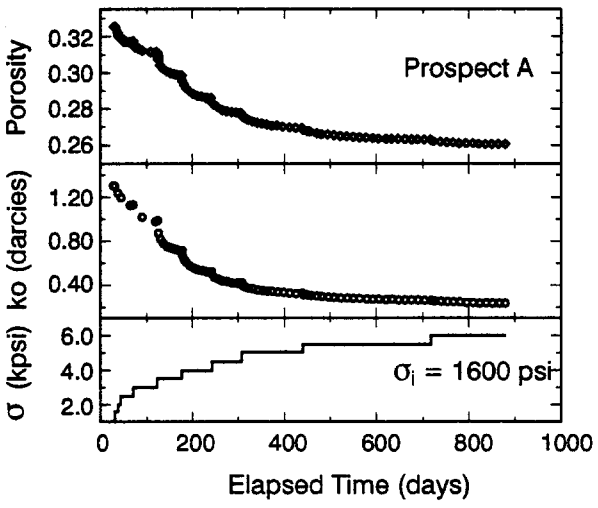

Fig. 3.48 Porosity and permeability versus time in response to applied effective stress (Ostermeier 1993)

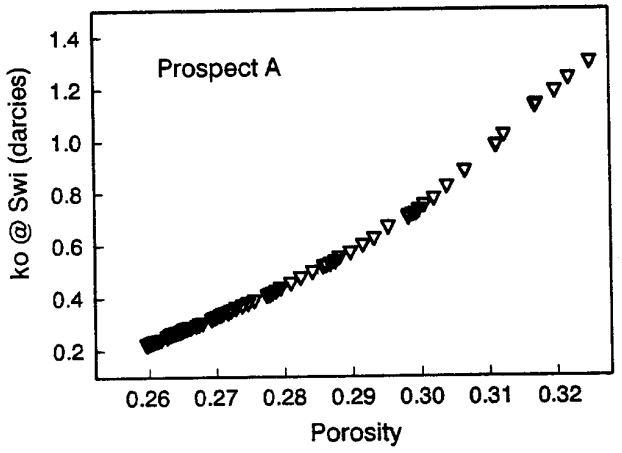

Fig 3.49 Oil permeability at Swi versus porosity (Ostermeier 1993)

Electrical Properties of Fluid Saturated Rock

The common method of determining the presence and saturation of hydrocarbon in a well is electrical logging for the formation electrical resistance. This is usually done before a well is cased but an observation well can be cased with a fiberglass casing. The basic principle of resistivity logging is that brine will conduct electricity but oil and most minerals are insulators. The amount of minerals present (i.e., 1 - porosity) is independently estimated by means such as acoustic logging. We will see that the electrical conductivity of fluid saturated rock is a function of porosity and tortuosity similar to permeability but differs from permeability in that it is not a function of the pore size.

Fig. 3.50 illustrates the major considerations in the conduction of an electrical current through fluid saturated rock. As electrical charges move through a homogeneous, isotropic, conductive medium possessing neither inductive or capacitive reactance, the electrical potential difference, *V*(volts), and the conductance, *c*(siemens), determine the intensity of charge movement per unit time, *I* (amperes). That is,

$$I = cV$$

The extrinsic conductance, *c*, of the medium is related, in turn, to its intrinsic conductivity, *C*, and its dimensions through the expression

$$c = \frac{C\,A}{L}$$

where *C* is the medium's conductivity (siemens/meter), *A* is its area (m^2), and *L* its length (m). These expressions can be combined as

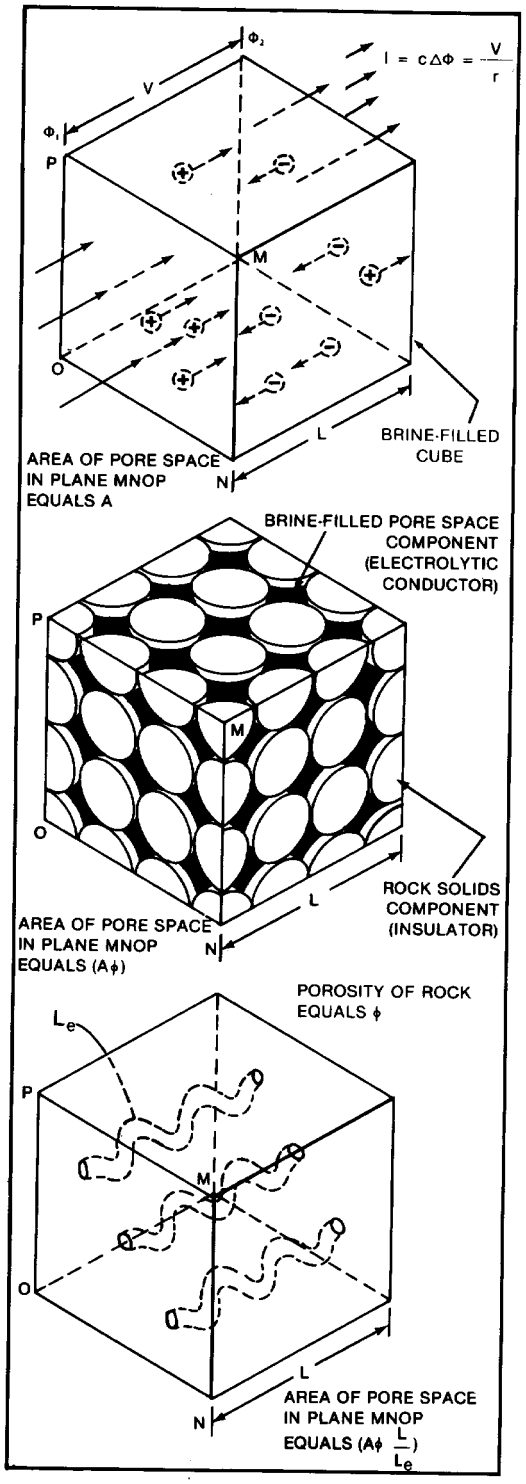

Fig. 3.50 Jorden and Campbell, 1986

$$I = V\left(\frac{C\,A}{L}\right)$$

$$\frac{I}{A} = C\frac{V}{L}$$

to relate current, potential difference, and conductivity for a homogeneous, isotropic, conductive medium. Note the parallel between this equation for the flux of electrical current as a function of a electrical potential gradient with the conductivity as the transport coefficient and Darcy's law which expresses volumetric flux as a function of the pressure gradient with the permeability divided by viscosity as the transport coefficient.

Pore Structure

The flow of electrical current through reservoir or aquifer rock is not through a homogeneous medium. The electrical current is through a composite medium consisting of a conducting brine phase, an insulating hydrocarbon or air phase, mineral phases that generally are insulating, and a brine saturated clay that may be more highly conductive that the brine alone. We will first consider the effect of porosity and pore structure on the electrical conductivity of a 100% brine saturated medium in the absence of clays.

Refer to a block of the composite medium with a cross sectional area of *A* and a length of *L* as illustrated in Fig. 3.50. The conductance, c_o, of the 100% brine saturated medium will be expressed in terms of its *conductivity,* C_o.

$$c_o = \frac{C_o\,A}{L}$$

The conductance of the medium is equal to the contribution of the conductivity of the brine in the pore spaces of the medium. The length of the conductive paths through the medium will be greater than *L* and it will be denoted as L_e. The effective cross sectional area for conduction is also reduced by the presence of the insulating solid. I believe the effective cross sectional area should be $A\phi$ but those who adhere strictly to the bundle of capillary models claim that the effective cross sectional area should be $A¢(L/L_e)$. I will use the latter convention to be consistent with the literature. The contribution of the brine to the conductance can be expressed as follows.

$$c_o = \frac{C_w\,A\phi\left(L/L_e\right)}{L_e}$$

where C_w is the conductivity of the brine (measured at appropriate temperature with a brine of the same electrolyte composition) and L_e is the effective length due to the tortuosity of the pores. If we assume that the brine is the only contributor to the conductance, we can equate the last two equations and solve for C_o.

$$C_o = \left(L / L_e\right)^2 \phi \; C_w$$
$$= \frac{\phi}{\tau_e} C_w$$

where τ_e is the ***tortuosity*** (or the square of the tortuosity). This equation can also be expressed in terms of the ***resistivity*** which is the reciprocal of the conductivity.

$$R_o = F_R \, R_w$$

where the ratio τ_e/ϕ has been combined into a single parameter, F_R, called the ***formation resistivity factor.***

$$F_R = \frac{\tau_e}{\phi}$$

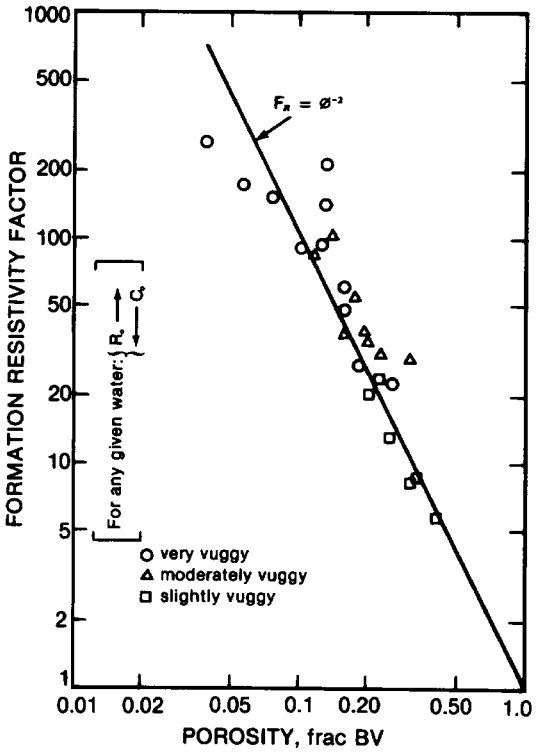

Fig. 3.51 Dependence of the formation resistivity - factor on porosity (Jorden and Campbell 1986)

This factor is the proportionality constant between the formation resistivity at 100% water saturation and the brine resistivity. It is a function of porosity and other features of the pore structure. Fig. 3.51 plots some measured formation resistivity factors as a function of the porosity. It appears to correlate with the inverse second power of the porosity. This implies that τ_e is approximately inversely proportional to the porosity. A tortuosity of 2.0 for a sand pack having a porosity of 0.4 is close to the tortuosity of 25/12 that we used for the Blake-Kozeny model of permeability. However, this correlation implies that the tortuosity will be equal to 10 for a rock with a porosity of 0.10. A literal interpretation of tortuosity means that the effective pore length is $\sqrt{10}$ times the medium length for a porosity of 0.10. This interpretation appears questionable. Owen (1952) modeled the porous medium as consisting of pore throats and pore bodies as illustrated in Fig. 3.52. The ***constriction factor****, F_c, is* the ratio of the size of the pore body to the pore throat, i.e., the *aspect ratio* of the porous medium. The pore throat and pore body are in series and a value of F_c greater than unity will result in a contribution of resistances in series to the formation factor. Fig. 3.53 plots the calculated formation factor as a function of the constriction factor, porosity, and tortuosity. These calculations shows that the effect of resistances in series are very significant when the aspect ratio is large.

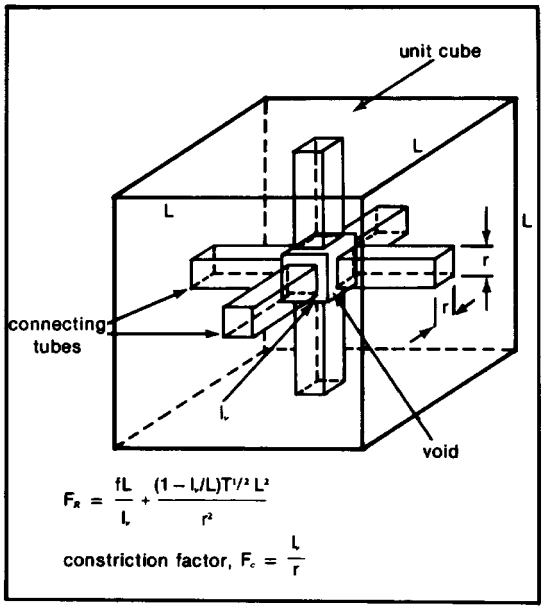

Fig 3.52 Model of porous medium containing pore bodies and pore throats of different sizes, [Jorden and Campbell 1986 (Owen 1952)]

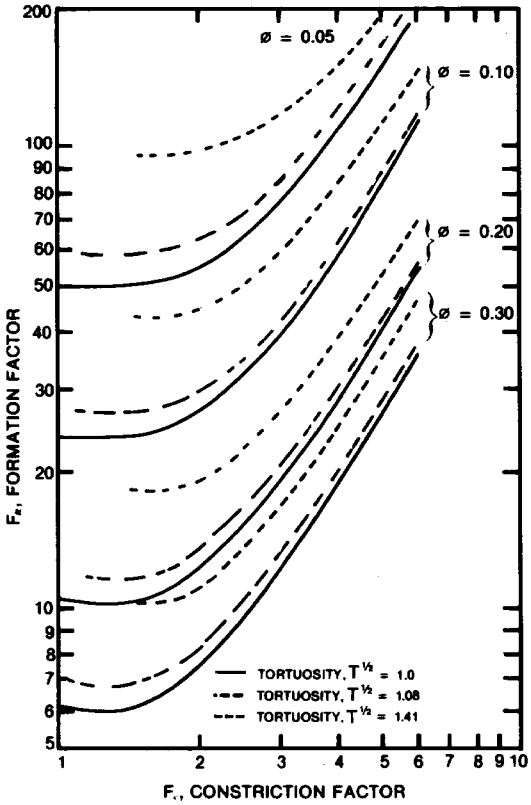

Fig 3.53 Relationship between formation resistivity factor and constriction factor for model in Fig. 3.52 [Jorden and Campbell 1986 (Owen 1952)]

These calculations also may offer means for estimating the aspect ratio from measurements of the formation factor. We will see later that the aspect ratio is an important factor in the trapping of a nonwetting phase. If we were to compare Fig. 3.51 with 3.53 while assuming a tortuosity of unity, the constriction factor will increase with decreasing porosity as follows.

Porosity	F_R	$\phi F_R = \tau_e$	Constriction factor
0.30	7	2	2
0.20	30	6	4
0.10	80	8	5
0.05	400	20	>6

This table shows that resistance in series becomes more important as the porosity decreases and this accounts for the large formation factors at low porosity.

Permeability Model Revisited

We determined here a tortuosity based on the electrical resistance of a brine saturated rock. Earlier we determined a tortuosity based of the hydraulic resistance to flow. We will now compare the equations and typical values for the two models of tortuosity.

$$\tau_e = \phi\, F_R, \qquad \text{electrical}$$

$$\tau = \frac{\phi^3\, D_p^2}{72\, k\, (1-\phi)^2}, \qquad \text{hydraulic}$$

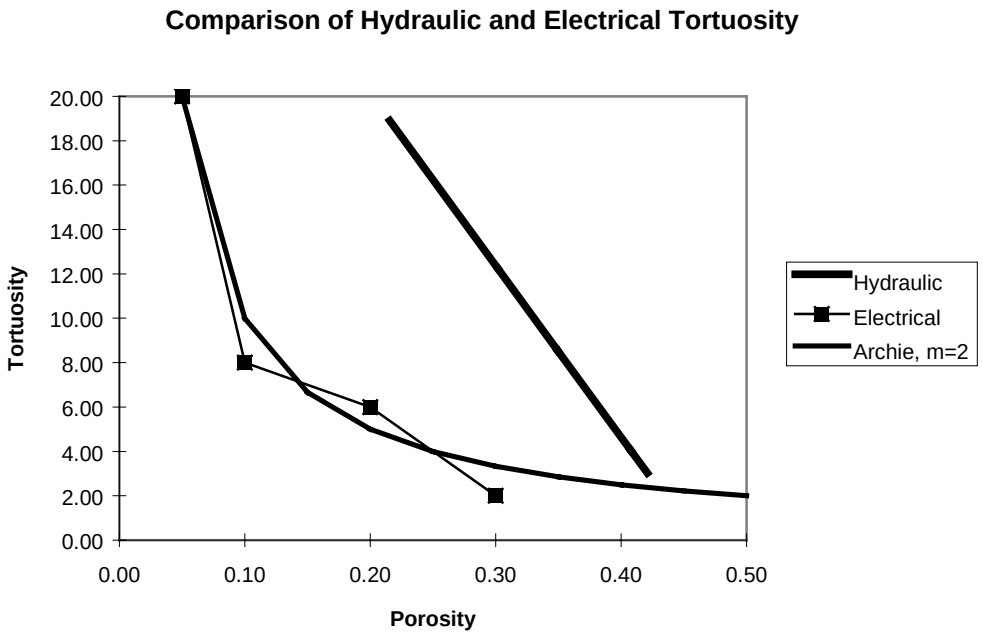

Fig. 3.54 Comparison of the tortuosity determined from permeability of unconsolidated sand with the tortuosity determined from electrical resistivity

Fig. 3.54 shows the hydraulic tortuosity to be much larger than the electrical tortuosity. Thus one should be cautioned to not assume that they are equal. Both models were based on a bundle of capillary tubes. The constrictions in the pores may have a greater effect on hydraulic resistance than it does on electrical resistance. This may be expected since hydraulic flow depends on the fourth power of pore throat diameter while electrical current depends on the second power of the pore throat diameter.

Archie Model

The formation resistivity factor as a function of porosity in Fig. 3.51 showed that the formation resistivity factor is approximated by a power law dependence on porosity. Fit of experimental data is facilitated by the Archie model (commonly referred to as Archie's law for brine saturated rock)

$$F_R = \phi^{-m}$$

where *m* is the ***lithologic exponent***. It often has a value near 2.0. However, Fig. 3.55 shows that vuggy rocks can have formation resistivity factors that do not have a power law behavior with an intercept of unity at unit porosity. Thus a modified Archie model which may better fit data over a limited interval is

$$F_R = K_R \phi^{-m}$$

where K_R is the ***formation resistivity factor coefficient***.

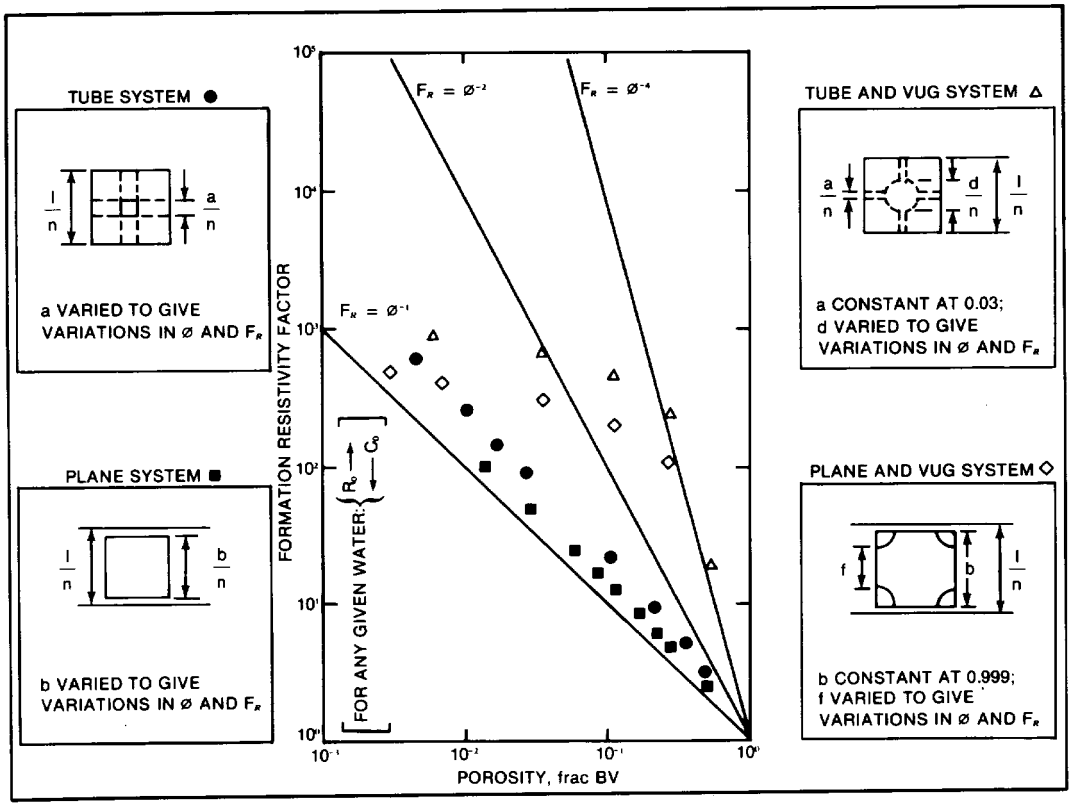

Fig. 3.55 Relationship between formation resistivity factor and porosity for some model pore systems [Jorden and Campbell, 1986 (Towle, 1962)]

Effect of Clays

The model of the conductivity developed so far has the formation conductivity proportional to the brine conductivity with the constant of proportionality equal to the reciprocal of the formation resistivity factor.

$$C_o = \frac{1}{F_R} C_w$$

in the absence of clays.

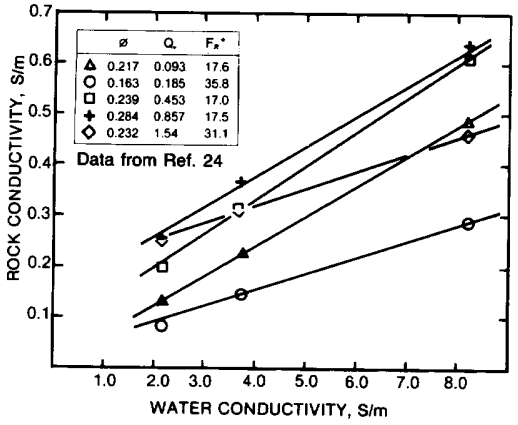

F_R^* is shaly sand formation resistivity factor

Q_v is cation exchange capacity per unit PV

Fig. 3.56 Effect of clay content and water conductivity on electrical conductivity of 100% water-saturated rock (Jorden and Campbell, 1896)

Figure 3.56 shows that the rock sample with a low **cation exchange capacity** per unit pore volume, Q_v ,(proportional to clay content) indicated by triangles does appear to have a conductivity that is proportional to the brine conductivity, i.e., has a zero intercept. However, as the value Of Q_V increases, the intercept increases. The intercept is given as a function of Q_V below. Thus, some correction of Archie's law is needed for the case of rocks having a significant amount of clays.

Q_v	$C_o@C_w=0$
0.093	0.00
0.185	0.02
0.453	0.06
0.857	0.12
1.54	0.19

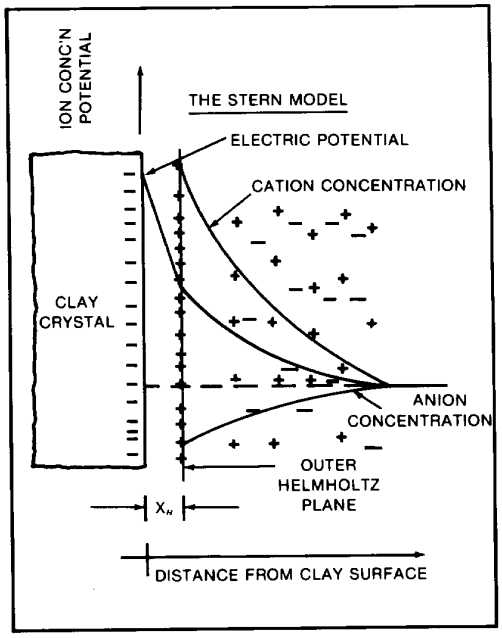

Fig. 3.57 The electrical charge distribution near clay surfaces (Jorden and Campbell, 1986)

So far we have treated the brine as the only conductive material and assumed that it had homogeneous properties given by C_W. If we were to take a microscopic look into the brine filled pore space, we will find that the composition of the brine is different next to the clay surfaces. As a result of the electrical charges on the surfaces of the clays, we may see an ionic concentration profile as in Fig. 3.57. The negative charge on the clay surfaces is balanced by a net excess of cations (positive) and deficiency of anions (negative). This is called an electrical double layer because the layer of charge on the surface is balanced by the layer of charge in the solution in the vicinity of the surface. Usually the excess of cations is much greater than the deficiency of anions. If the electrolyte concentration in the brine is low, the ionic concentration in the double layer may be much greater than in the bulk solution. Since the conductivity is

approximately proportional to the ionic concentration, the double layer will be much more conductive than an equal volume of bulk solution. Thus the electrical double will act as a conductor in parallel with the bulk solution if the clays form a connected path through the medium. When conductors are in parallel their total conductance is equal to the sum of the individual conductance. Waxman and Smits introduced a model in 1968 that takes into account contribution due to the conductance of the clays.

$$C_o = \frac{1}{F_R^*}\left(B Q_v + C_w\right)$$

where
B = the equivalent ionic conductance of the cations in the electrical double layer, $cm^3/meq \cdot \Omega \cdot m$
Q_v = the cation exchange capacity per unit pore volume, meq/cm^3,
F_R^* = shaly sand formation resistivity factor

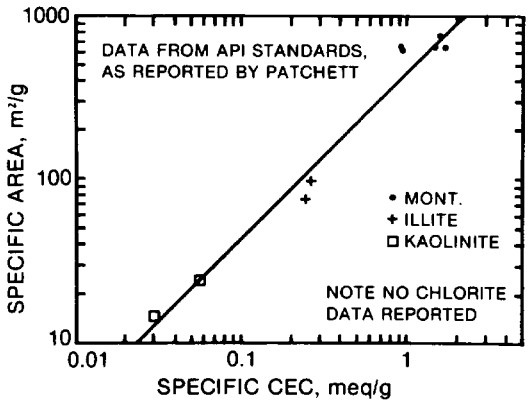

Fig. 3.58 Relationship between specific surface area and specific CEC for standard clays [Jorden and Campbell 1986 (Clavier et al. 1984)]

This equation for the conductivity of shaly sands takes into account the nonzero intercept observed in the shaly sands shown in Fig. 3.56. The cation exchange capacity per unit weight of disaggregated rock, *CEC* (meq/g), is measured by standard analytical methods. The fact that it is a surface effect can be seen from the linear correlation of the specific *CEC* with the specific area of some common clays in Fig. 3.58.

Assignment 3.6 Cation Exchange Capacity Calculate the area (nm^2) per charge on clay surfaces from the data on Fig. 3.58. An equivalent is an amount of material corresponding to Avogadro number (6.0238×10^{23}) of positive and negative charges.

Hydrocarbon Saturation

So far we have discussed the conductivity or resistivity of 100% brine saturated rock. The presence of a nonconductive hydrocarbon occupying a portion of the pore space will result in a decrease in the conductivity. To estimate the hydrocarbon saturation we need to determine how much the rock conductivity is reduced by the presence of the hydrocarbon. Archie found that for clay-free rock the reduction of the rock conductivity due to the presence of hydrocarbon could be described with a power-law model similar to the dependence of the formation resistivity factor on porosity (Archie's law for partially brine saturated rock).

$$R_t = I_R R_o$$

and

$$C_t = \frac{1}{I_R} C_o$$

where R_t and C_t are the resistivity and conductivity, respectively, of the partially water saturated rock and I_R is the ***hydrocarbon resistivity index***. When the hydrocarbon resistivity index follows the power model, it can be described as

$$I_R = S_w^{-n}$$

where n is the ***saturation exponent***. Fig. 3.59 shows the hydrocarbon resistivity index as a function of water saturation (called I - S_w plot) for rocks with different wettability. The data with preferentially water-wet and neutral wettability conditions do have a power law behavior with a saturation exponent about 2.0 for neutral wettability and less than 2.0 for preferentially water-wet. The samples that are preferentially oil wet deviate significantly from the power law behavior with an exponent of 2.0. When the rock is water-wet the water remains connected as the water saturation reduces and the reduction in conductivity is due to increased tortuosity and resistances in series similar to the models for the formation resistivity factor. However, when the rock is preferentially oil-wet, the water becomes disconnected as the water saturation decreases and the disconnected water contributes nothing to the conductivity. Thus the resistivity increases much more rapidly as water becomes disconnected.

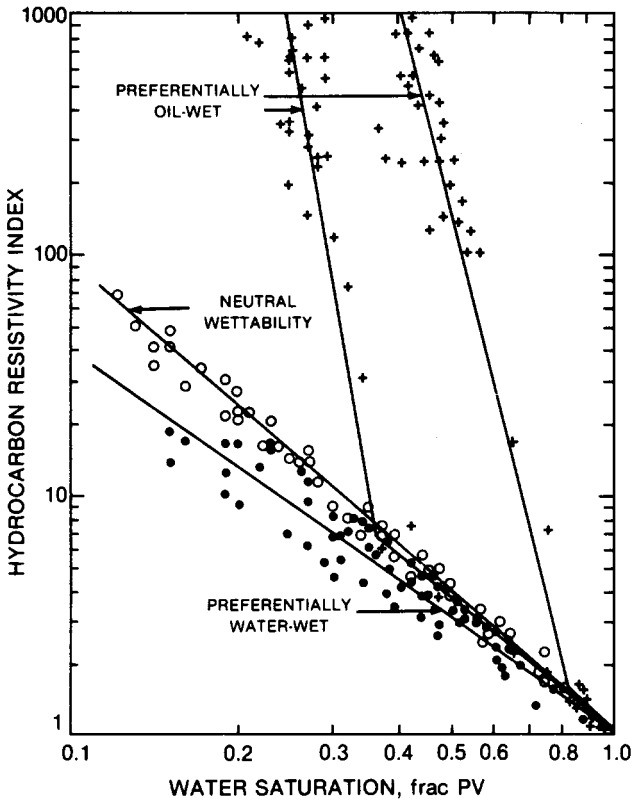

Fig. 3.59 Effect of wettability on hydrocarbon resistivity index of carbonates [Jorden and Campbell 1986 (Sweeney and Jennings 1960)]

Earlier we saw that in the presence of a significant amount of clays, the formation resistivity factor given by the Archie model had to be modified as in the Waxman-Smit model. When hydrocarbon is present in shaly sands the Archie model is modified by the Waxman-Thomas model.

$$C_t = \frac{1}{F_R^*}\left(\frac{1}{S_w^{1-n^*}} B Q_v + \frac{1}{S^{-n^*}} C_w\right)$$

Electric Logging

Electrical logging for formation evaluation is the recording of one or more electrical properties in a well by lowering a logging tool into the well on a wire line. The usual measurements are the spontaneous potential (SP) and resistivity (or conductivity) logging. Fig. 3.60 is an example of an electrical log in a sandstone formation. The resistivity tools with different electrode spacing measures resistivity averaged over different volumes the formation. Notice that the tools with wider spacing has higher resistivity as there is less flushing by the drilling mud filtrate deeper into the formation.

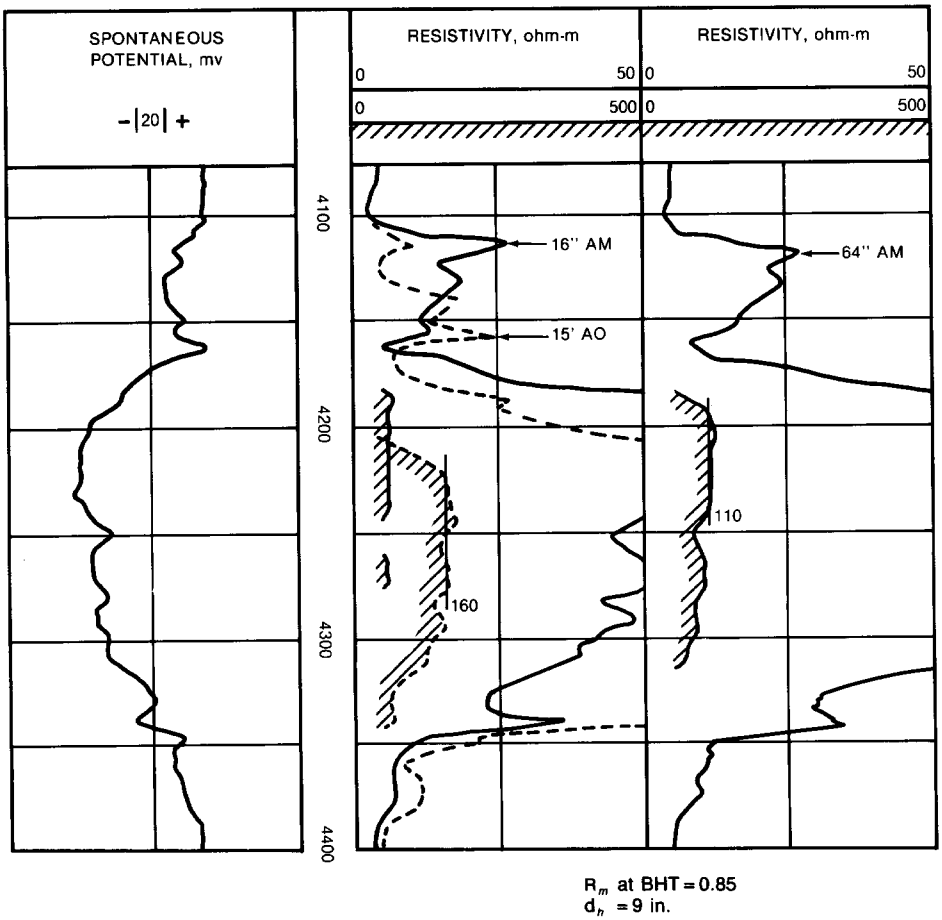

i. . . The bed is very thick and reasonably homogeneous, although the slightly dissymmetrical shapes of the SP and normal resistivity curves, and also several ripples in the curves, indicate the presence of shale streaks, mostly in the lower part.

Since the formation is known to be reasonably porous, and the connate water to be highly mineralized. the high resistivity obtained with the long normal and the lateral can be interpreted as significant of high oil saturation.

. .. No maximum is noticed with the lateral near the lower boundary of the bed, which is due to the progressive increase of shaly material downwardly ..

The bed can be considered as infinitely thick with respect to the spacing of the long normal (e = 70'). On the other hand, according to the lithologic characteristics of the bed, the value of R,/R,,, should be taken at least equal to 20, and the penetration of mud filtrate is certainly rather deep . . ."

Fig. 3.60 Example conventional electrode log - consolidated sandstone (Jorden and Campbell, 1986)

References

Aitchison, J. and Brown, J. A. C.: The Lognormal Distribution, Cambridge Press, London, 1957.

Bear, J.,: Dynamics of Fluids in Porous Media, Dover Publications, New York, 1 972.

Bird, R. B., Stewart, W. E., and Lightfoot, E. N.: Transport Phenomena, John Wiley & Sons, New York, 1960.

Beard, D. C. and Weyl, P. K.: “Influence of Texture on Porosity and Permeability of Unconsolidated Sand,” AAPG Bull., Vol. 57, No. 2, (1973), 349-369.

Bjorlykke, K.: Sedimentology and Petroleum Geology, Sorinaer-Verlag, York, 1989.

Collins, R. E.: Flow of Fluids through Porous Materials, Reinhold Publishing Corp., NewYork,1961.

Corey, A. T.: Mechanics of Immiscible Fluids in Porous Media, Water Resources Publications, Littleton, CO, 1986.

Jorden, J. R. and Campbell, F. L.: Well Logging I - Rock Properties. Borehole Environment. Mud and Temperature Logging, SPE of AIME,1984.

Jorden, J. R. and Campbell, F. L.: Well Logging II - Electrical and Acoustic Logging, SPE of AIME, 1986.

Ma, S., Jiang, M.-X., and Morrow, N. R.: “Correlation of Capillary Pressure Relationships and Calculations of Permeability,” SPE 22685 presented at the 66th ATCE of SPE, Dallas, TX, Oct. 6-9, 1991.

Ostermeier, R. M.: "Some Core Analysis Issues Related to Deep Water Gulf of Mexico Turbidites", Society of Core Analysts conference paper no. 9315, Aug. 911,1993.

Ostermeier, R.M.: "Stressed Oil Permeability of Deepwater Gulf of Mexico Turbidite Sands: Measurements and Theory," SPE 30606 prepared for presentation at the 70th ATCE of SPE, Dallas, TX, Oct. 22-25, 1995.

Panda, M.N. and Lake, L.W.: "Estimation of Single-Phase Permeability from Parameters of Particle-Size Distribution," AAPG Bulletin, Vol. 78, No. 7 (July 1994), 1028-1039.

Purcell, W. R.: "Capillary Pressures - Their Measurement Using Mercury and the Calculation of Permeability Therefrom", Pet. Trans. AIME, Feb., 1949, 39-48.

Scheidegger, A. E.: The Physics of Flow Through Porous Media, University of Toronto Press, Toronto, 1957.

Selley, R. C.: Petroleum Geology, W. H. Freeman & Co., New York,1985.

Swanson, B. F.: “A Simple Correlation Between Permeabilities and Mercury Capillary Pressures,” J. Pet. Tech. (Dec. 1981), 2498-2504.

Swanson, B. F.: ‘Microporosity in Reservoir Rocks: Its Measurement and Influence on Electrical Resitivity,” The Log Analyst, (Nov. - Dec. 1985), 42-52.

"The Sl Metric System of Units and SPE Metric Standard", SPE of AIME, Dallas, 1984.

Thomeer, J. H. M.: “Introduction of a Pore Geometrical Factor Defined bt the Capillary Pressure Curve,” J. Pet. Tech. (March, 1960), 73-77.

Thomeer, J. H. M.: “Air Permeability as a Function of Three Pore-Network Parameters,” J. Pet. Tech. (April 1983), 809-814.